Ecological Indicators 121 (2021) 107107

Contents lists available at ScienceDirect

Ecological Indicators

journal homepage: www.elsevier.com/locate/ecolind

Quantitative analysis of nonlinear climate change impact on drought based on the standardized precipitation and evapotranspiration index

Ruxin Zhao [a], Huixiao Wang [a,*], Ji Chen [b], Guobin Fu [c], Chesheng Zhan [d,e], Huicai Yang [f]

[a] Beijing Key Laboratory of Urban Hydrological Cycle and Sponge City Technology, College of Water Sciences, Beijing Normal University, Beijing 100875, China
[b] Department of Civil Engineering, The University of Hong Kong, Pokfulam, Hong Kong, China
[c] CSIRO Land and Water, Private Bag 5, Wembley, WA 6913, Australia
[d] Key Laboratory of Ecosystem Network Observation and Modeling, Institute of Geographic Sciences and Natural Resources Research, Chinese Academy of Sciences, Beijing 100101, China
[e] Yucheng Comprehensive Experiment Station, Chinese Academy of Science, Beijing 100101, China
[f] School of Land Resources and Urban and Rural Planning, Hebei GEO University, Shijiazhuang 050000, China

ARTICLE INFO

Keywords:
Climate change
Nonlinear change
SPEI
Relative contribution
Drought

ABSTRACT

Exploring the impact of climate change on drought under changing environmental conditions is crucial for agriculture, ecology, and human society. To evaluate the role of climate change on drought, this study selected the Songnen Plain (SNP) in Northeast China as a study area in which to quantify the relative contributions of climatic variables to the drought trend in accordance with the Standardized Precipitation and Evapotranspiration Index (SPEI). A series of SPEI-based numerical experiments, using combinations of observational and nonlinear detrended climatic variable data series, was used as a synthetic approach with which to analyze the relative impact of the individual climatic variables. Results indicated that drought on the SNP has been mitigated marginally during 1961–2016, mainly during spring, winter, the growing season, and on the annual timescale. Significant trends were detected in relation to temperature, sunshine duration, and wind speed, and these variables had differing roles in drought evolution. An increasing trend in temperature was found to aggravate drought tendency at all investigated timescales; however, decreasing trends in net radiation and wind speed offset the drought tendency caused by rising temperature. The positive contribution of wind speed was larger than the negative contribution of temperature, especially in areas around 46°N. Although the change of precipitation was not significant, it promoted drought mitigation on the SNP in spring, winter, the growing season, and on the annual timescale. The analysis framework used in this study was shown useful for improving understanding of the relationship between climate change and drought evolution, and it could prove helpful in providing rational and regulatory policy strategies regarding drought relief.

1. Introduction

Increasing attention is being paid to the consequences of climate change owing to their profound impact on natural ecosystems and human society (Guzman-Morales and Gershunov, 2019; Tang, 2019). One of the effects of climate change is intensification of the hydrological cycle, which means that the magnitude, frequency of occurrence, and extent of the area affected by related extreme climatic events are predicted to increase (Dai, 2011). Drought is one such extreme event that occurs frequently in almost all climatic regimes with observed trends of warming (Dai, 2013; Carrão et al., 2018). Recent work has suggested that warming trends are expected to continue into the future (Pachauri et al., 2014). For a given basin, an increase in temperature might accelerate the evaporative demand and increase both the occurrence and the uncertainty of extreme precipitation (Easterling et al., 2007; Allan and Soden, 2008; Giorgi et al., 2019; Papalexiou and Montanari, 2019), which could lead to differences in the worldwide pattern of distribution of drought. Thus, it is very important to investigate the mechanism of drought, within the context of a changing environment, owing to its detrimental effects on agricultural production (Lobell et al., 2011), ecological systems (Li et al., 2019), and socioeconomic security and stability (Hsiang et al., 2013).

* Corresponding author at: No. 19, Xueyuannan Road, Xinjiekouwai Street, Haidian District, Beijing 100875, China.
E-mail addresses: zhaorx324@163.com (R. Zhao), huixiaowang@bnu.edu.cn (H. Wang), jichen@hku.hk (J. Chen), Guobin.Fu@csiro.au (G. Fu), zhancs@igsnrr.ac.cn (C. Zhan), Huicai.Yang@hgu.edu.cn (H. Yang).

https://doi.org/10.1016/j.ecolind.2020.107107
Received 28 May 2020; Received in revised form 24 August 2020; Accepted 19 October 2020
Available online 5 November 2020

The occurrence of drought, which is the result of water deficit over a long period, is relative to the moisture supply (precipitation) and the moisture fluxes from the surface to the atmosphere (evapotranspiration). Globally, both precipitation and evaporative demand are expected to increase under the conditions of a warming climate (Huntington, 2006; Trenberth, 2011; Cook et al., 2014). Regionally, however, the increase in precipitation is predicted to occur mainly via heavy or extreme precipitation events and primarily in mesic areas, resulting in a "rich-get-richer/poor-get-poorer" scenario (Cook et al., 2014). Contrary to the expectation that evaporative demand would increase with global warming, both observed pan evapotranspiration and estimated potential evapotranspiration (PET) demonstrate a decreasing tendency in the United States (Irmak et al., 2012), Australia (Donohue et al., 2010), northeastern India (Jhajharia et al., 2012), southeastern Turkey (Ozdogan and Salvucci, 2004), and China (Liu, 2004; Zhang et al., 2019a). This "pan evaporation paradox" phenomenon suggests that evapotranspiration change is not controlled primarily by temperature, but is susceptible to variation of other meteorological variables on seasonal–decadal scales. Zhang et al. (2019a) suggested that maximum temperature, relative humidity, and wind speed are the major controlling factors affecting PET change over China, while Jiang et al. (2019) indicated that PET change in Southwest China is most sensitive to relative humidity, followed in descending order by sunshine duration, temperature, and wind speed. The mechanism of drought is complex due to the various interactions among different components within the system, such as soil moisture, evapotranspiration, precipitation, and anthropogenic-related warming (May et al., 2017; Samaniego et al., 2018; Teuling, 2018). Therefore, an in-depth impact assessment of the different factors affecting drought is necessary for better understanding the drought mechanisms.

Previous related studies have explored the impact of climate change on drought (Li and Sun, 2017; Sun et al., 2017; Sun and Ma, 2015; Zhang et al., 2016; Zhang et al., 2019b). Cook et al. (2014) indicated that the expansion in the global area of drought by 2080–2099 would be attributable to increased PET. Williams et al. (2015) separated the contributions of individual meteorological variables in relation to the California drought of 2012–2014 and found that anthropogenic warming accounted for 8–27%. Chen and Sun (2017) suggested that external natural forcing is mainly responsible for the variability of drought in China but that anthropogenic activity influences drought trend of increase. Zhang et al. (2016) conducted quantitative investigation of the different impacts of the linear changes in climatic variables on drought, and found that rising temperature was the main forcing for the drought trend throughout China, then followed by decreasing wind speed and sunshine duration. Wu and Chen (2019) proposed a simple algorithm for quantification of the individual contributions of the linear changes in temperature and precipitation to the dryness/wetness trend in the Pearl River Basin in southern China. Their findings indicated that temperature change had greater effect than precipitation change. The approaches used in the above research on the impact of climate change on drought mostly considered linear detrending of the variables (Zhang et al., 2016; Wu and Chen, 2019), and the timescale over which the variables were detrended was generally monthly (Li and Sun, 2017; Wu and Chen, 2019) or annually (Zhang et al., 2016). However, climatic variables will not necessarily change with the same trend over long periods (Li et al., 2015). To obtain greater insight into the relationship between climate change and drought, it is important to reveal details by exploring the extent to which fine-scale climate change is relevant to drought at broader scales. Therefore, an empirical mode decomposition approach was used in this study to detrend the nonlinear trends of climatic variables at the daily timescale, which were then used to investigate the impact of the individual climatic variables on drought at longer timescales.

As an example of the impact of drought on agriculture, after 1980 s the absolute loss of grain was increased by 200–450 $\times$ 10^4 t in Northeast China and provinces such as Shanxi, Hubei, and Guizhou (Zhang et al., 2015). Northeast China, which is a major food production base with a cultivated area of six million hectares, has experienced more frequent and intensified drought events since the 1990 s (Jiang et al., 2018; Xia et al., 2018). The Songnen Plain (SNP), which is the main grain production center of Northeast China, experienced a drying process in the previous century because of the expansion of the area of cultivated land (Zhang et al., 2018a) and the frequent occurrence of spring drought (Song et al., 2014). Several recent studies investigated the spatiotemporal changes of drought on the SNP (Kang and Zhang, 2016; Yang et al., 2017; Zuo et al., 2019), and others discussed the relationships between drought and certain controlling factors, e.g., extreme temperature and precipitation (Guo et al., 2019b), soil moisture (Meng et al., 2019), PET (Ma et al., 2017), and pan transpiration (Liang et al., 2011). However, quantification of the relative contributions of such climatic variables to drought on the SNP has been overlooked.

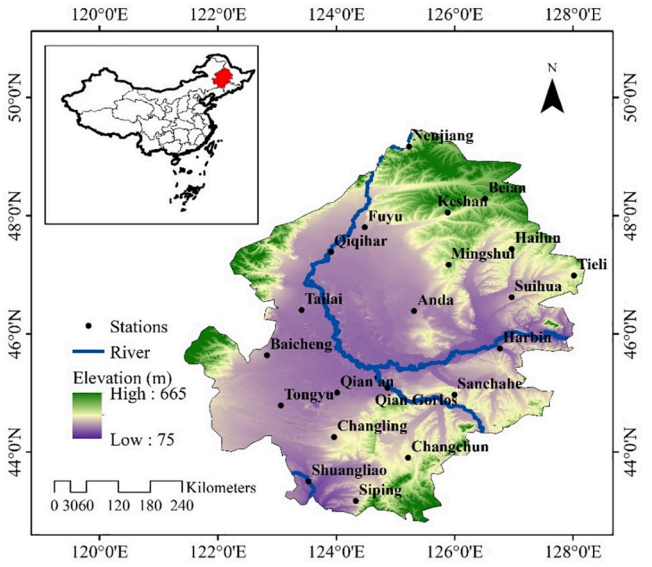

Fig. 1. Location of meteorological stations on the Songnen Plain.

A further consequence of extended meteorological drought is the occurrence of hydrological drought, agricultural drought, and even socioeconomic drought (Leng et al., 2015). Therefore, the objective of this study was to quantify and explicitly separate the relative contributions of the changes in different climatic variables to the tendency of meteorological drought on the SNP at different timescales. To achieve this purpose, we designed a series of numerical experiments based on the Standardized Precipitation Evapotranspiration Index (SPEI; Vicente-Serrano et al., 2010) that used daily data of certain meteorological variables from 21 meteorological stations (1961–2016) and a nonlinear detrending method. The SPEI provides a flexible means for estimation of the surface moisture balance, and it makes it possible to vary the inputs (e.g., precipitation, temperature, and net radiation) to separate and quantify the effect of specific variables on drought trend. Specifically, our study addressed the following three questions in relation to the SNP. (1) Which specific climatic variables changed significantly during the study period? (2) What has been the spatiotemporal distribution of meteorological drought in recent years? (3) What were the relative contributions of the significantly changed climate variables to the current drought tendency?

2. Material and methods

2.1. Study area

The SNP lies in the region 42°48′–49°28′N, 121°24′–128°10′E, and it covers an area of 22.35 $\times$ 10^4 km^2 that has elevation of 75–665 m

(Fig. 1). Cultivated land accounts for 58% of the SNP, which represents 8% of the total area of cultivated land in China. Spring maize, soybean, and spring wheat are the main crops grown in this region. The SNP is dominated by a temperate continental monsoon climate, and it has clear seasonality with cold/dry winters and hot/wet summers influenced by the southeast monsoon. Average temperature varies from − 19 ℃ in January to 23 ℃ in July. Annual precipitation is in the range of 300–600 mm (Chen et al., 2011b). Mean annual PET in the SNP increases from northeast to southwest with values of < 850 to > 1100 mm, respectively (Ma et al., 2017).

2.2. Data

The daily meteorological datasets (1961–2016) used in this study, obtained from the China Meteorological Data Sharing Service System (http://data.cma.cn/), represented 21 meteorological stations distributed evenly across the SNP (Fig. 1). The major meteorological variables considered were maximum temperature (Tmax, ℃), average temperature (Tave, ℃), minimum temperature (Tmin, ℃), precipitation (P, mm), air pressure (Pr, hPa), wind speed at 2 m above ground level (U_2, m/s) that was converted from the 10-m wind speed using a standard conversion formula (Allen et al., 1998), sunshine duration (Sd, h), and relative humidity (RH, %). Missing data were filled via linear interpolation (Li and Sun, 2017) if the time gap was within 5 d; otherwise, they were replaced with the average values of those days in all other years.

2.3. Methodology

2.3.1. Selection of drought index

Drought indices are important tools that can be used for detection, monitoring, and quantification of drought events. However, owing to the complexity of drought, no single index can adequately capture the duration, severity, magnitude, and spatial extent of a drought event (Heim, 2002). The indices used most commonly in drought analysis are the Standardized Precipitation Index (SPI) (McKee et al., 1993), SPEI (Vicente-Serrano et al., 2010), and Palmer Drought Severity Index (PDSI) (Wells et al., 2004). In comparison with both the SPI and the PDSI, Wang et al. (2015) found that the SPEI has stronger correlation with soil moisture. One of the disadvantages of the PDSI is its fixed timescale, which limits its universal application because droughts are multiscalar phenomena (Mishra and Singh, 2010). Although the SPI can detect drought events at different timescales through simple calculation, its use of precipitation data as the only input can result in misestimation of the drought condition in certain regions, especially where evapotranspiration is greater than precipitation. Using the difference between precipitation and PET as input, the SPEI was developed as a generalized drought index that not only offers the same level of flexibility as the SPI, but also represents a simple climate water balance. The applicability of the SPEI to evaluation of drought events in different climatic regions has been validated in many earlier works (Liu et al., 2018; Nguvava et al., 2019; Wang et al., 2014; Zhang and Shen, 2019). Thus, the SPEI was selected as the drought metric for use in this study.

Precipitation and evapotranspiration are the main factors to consider when calculating the SPEI. Several equations are available for estimating PET based on theoretical and empirical models, e.g., the temperature-based Thornthwaite equation, temperature- and latitude-based Hamon equation (Hamon, 1961), radiation- and temperature-based Priestley–Taylor method (Priestley and Taylor, 1972), and Penman–Monteith equation (Allen et al., 1998), which is based on wind speed and humidity, as well as temperature and radiation. In comparison with other methods, the Penman–Monteith equation additionally incorporates both the energy balance and aerodynamics theory; thus, it is recommended as the sole standard method for accurate PET estimation by both the World Meteorological Organization (WMO, 2006) and the Food and Agriculture Organization of the United Nations (Allen et al., 1998). The SPEI was developed by Vicente-Serrano et al. (2010)

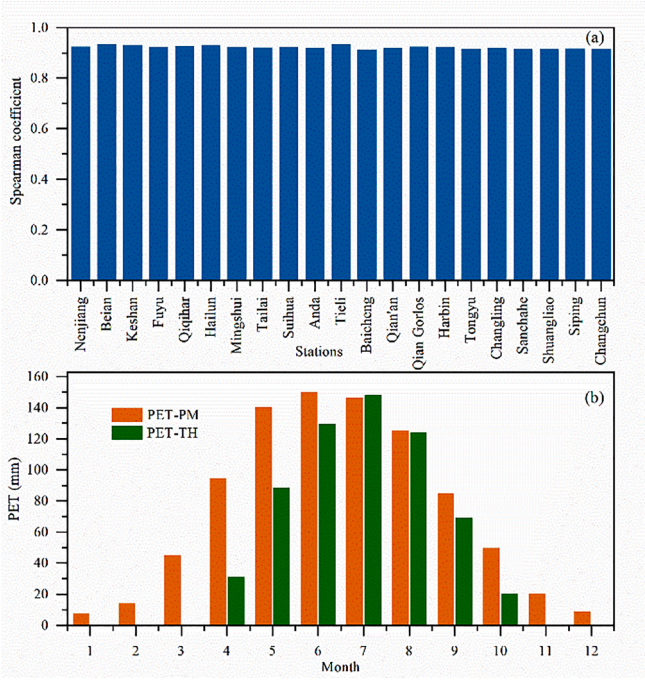

Fig. 2. Comparison of PET-PM and PET-TH.

using the Thornthwaite equation to calculate PET; however, it is inadvisable to estimate PET using a method based primarily on temperature (Jeong et al., 2014). We also compared the differences between the PET calculated using the Thornthwaite equation (PET-TH) and the PET calculated using the Penman–Monteith equation (PET-PM). Although their spearman coefficients at the 21 stations were all > 0.9 at the annual timescale (Fig. 2a), the PET-PM over the SNP was generally larger than the PET-TH, and the differences were reflected mainly in the colder months (Fig. 2b). Comparatively, the Penman–Monteith equation has been used most widely in previous studies and found to provide results that are most consistent, reliable, and accurate (Yin et al., 2010; Pereira et al., 2015; Li et al., 2017). If the data needed are available, the Penman–Monteith method is generally superior for estimation of PET (Beguería et al., 2014). Therefore, in this study, we used the Penman–Monteith method to calculate PET:

$$\mathrm{PET} = \frac{0.408\Delta(R_n - G) + \gamma \frac{900}{T+273} u_2 (e_s - e_a)}{\Delta + \gamma(1 + 0.34u_2)}, \quad (1)$$

where PET is the reference evapotranspiration (mm/d), Δ is the slope of the saturation vapor pressure curve at a given air temperature (kPa/℃), R_n is net radiation at the crop surface (MJ/(m^2.d)), G is the soil heat flux density (MJ/(m^2·d)), γ is the psychrometric constant (kPa/℃), T is the mean daily air temperature at 2-m height (℃), U_2 is the wind speed at 2-m height (m/s), e_s is the saturation vapor pressure (kPa), e_a is the actual vapor pressure (kPa), and ($e_s - e_a$) is the saturation vapor pressure deficit (kPa).

After calculating PET, the difference (D) between precipitation and PET can be aggregated at different timescales:

$$D_n^k = \sum_{i=0}^{k-1} P_{n-i} - PET_{n-i}, \quad (2)$$

where k is the timescale of the aggregation (e.g., 1-, 3-, 6-, and 12-months) and n is the calendar calculation month ($n = 1$ to 12).

For D values at different timescales, the cumulative distribution function of a three-parameter Log-logistic distributed variable can be calculated as follows:

$$F(x) = \left(1 + \left(\frac{\alpha}{x - \gamma}\right)^{\beta}\right)^{-1}, \quad (3)$$

where α, β, and γ are the scale, shape, and origin parameters, respectively.

Finally, the SPEI can be obtained by transforming $F(x)$ to a normal variable based on the classical approximation (Abramowitz and Stegun, 1965):

$$SPEI =$$

$$\begin{cases} w - \dfrac{c_0 + c_1 w + c_2 w^2}{1 + d_1 w + d_2 w^2 + d w^3}; if F(x) \geq 0.5, w = \sqrt{-2\ln(1 - F(x))} \\ -\left(w - \dfrac{c_0 + c_1 w + c_2 w^2}{1 + d_1 w + d_2 w^2 + d w^3}\right); if F(x) < 0.5, w = \sqrt{-2\ln(F(x))} \end{cases}, \quad (4)$$

where $c_0 = 2.51517$, $c_1 = 0.802853$, $c_2 = 0.010328$, $d_1 = 1.432788$, $d_2 = 0.189269$, and $d_3 = 0.001308$.

In this study, the SPEI at the 3-month timescale (denoted as $SPEI_3$) was used to reflect the seasonal drought condition. The $SPEI_3$ values in February, May, August, and November were taken as representative of the drought condition in winter, spring, summer, and autumn, respectively. The $SPEI_6$ value in September was used to represent the drought condition in the growing season. The $SPEI_{12}$ value in December was used to represent annual drought.

2.3.2. Nonlinear detrending method

The method of complete ensemble empirical mode decomposition with adaptive noise (CEEMDAN) was applied to decompose the meteorological variables during the period 1961–2016 into their nonlinear trends. The CEEMDAN approach is based on the methods of empirical mode decomposition (EMD) and ensemble empirical mode decomposition (EEMD), which are robust adaptive and temporal time series analysis methods often used for analyzing nonlinear and nonstationary components in climate data (Huang et al., 1998; Wu et al., 2009). Compared with EMD and EEMD, the major advantage of the CEEMDAN method is that it reduces the reconstruction error to minimum (or even zero) and reduces the noise in each intrinsic mode function, resulting in a complete and accurate decomposition for the raw data series (Colominas et al., 2014).

For a given target series $x(t)$, the CEEMDAN algorithm can be described as follows:

Step 1: Generate a new series $x^{(i)}$:

$x^{(i)} = x(t) + \beta w^{(i)}$, (5)where $\beta > 0$ and $w^{(i)}$ is a zero mean unit variance white noise realization ($i = 1, 2, \ldots, L$).

Step 2: Decompose completely each $x^{(i)}$ using EMD, following which the intrinsic mode function candidate $d_k^{(i)}$ ($k = 1, 2, \ldots, K$) is obtained. As the k-th mode of $x(t)$, $\overline{d_k}$ is obtained by averaging the corresponding modes $d_k^{(i)}$. Then, the first mode d_1 can be obtained:

$d_1 = \overline{d_k} = \frac{1}{L}\sum_{i=1}^{L} d_1^{(i)}$, (6)

Step 3: Separate the first residual r_1 from the given series $x(t)$:

$r_1 = x(t) - d_1$, (7)

Step 4: Use the first residual r_1 as the new target series, and repeat **Step 1** to **Step 3**. The second mode d_2 can be obtained and the second residual r_2 can be calculated as follows:

$r_2 = r_1 - d_2$, (8)

Therefore, the k-th ($k = 2, 3, \ldots, K$) residual is summarized as:

$r_k = r_{k-1} - d_k$, (9)

Step 5: Go to **Step 4** for the next k, until the obtained residual cannot be decomposed further using EMD. Then, K modes d_i and the final residual component r_k are obtained. Finally, the signal of $x(t)$ can be expressed as:

$x(t) = \sum_{i=1}^{K} d_k + r_K$, (10)where $x(t)$ is the raw data series, d_k is the k-th intrinsic mode function, which could also represent different periodic characteristics of $x(t)$, and r_K is the final residual component, which could represent the nonlinear trend of $x(t)$.

Based on the CEEMDAN results, a detrended data series x_d can be obtained by removing the nonlinear trend from the raw data series x. To ensure that the initial value of the detrended data series remains equal to the initial value of the raw data series, e.g., $x(1961)\_d = x(1961)$, the first value of the residual series r_K is added to the decomposed time series $\sum_{i=1}^{K} d_i$, which is addressed as described in previous studies (Sun and Ma, 2015; Li and Sun, 2017). Each daily climatic variable (except precipitation) on 365 calendar days per year (data on February 29 in a leap year were ignored) at the 21 stations was detrended using the CEEMDAN method. For precipitation, monthly data of the 12 calendar months per year at the 21 stations were detrended.

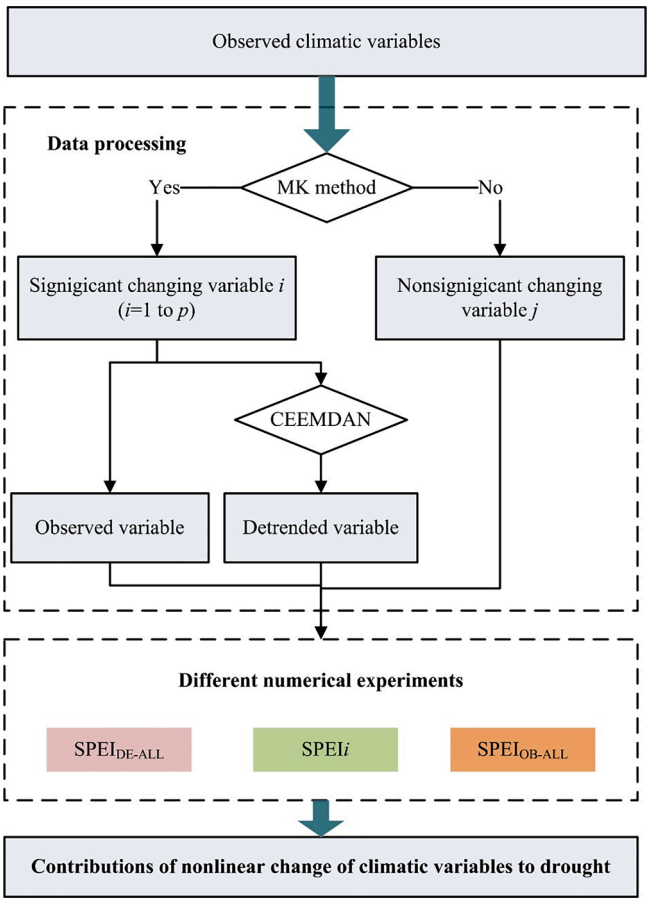

Fig. 3. General flow diagram of the procedure used to obtain the direct respective contributions of the meteorological variables to the trend of drought.

2.3.3. Trend analysis

The "Sen's slope" method (Sen, 1968) does not require a specific sample distribution nor is it influenced by outliers; therefore, we used it to reflect the magnitude of the trend of the climatic variables and the SPEI in the SNP region during 1961–2016. The equation can be expressed as follows:

$\beta = \text{Median}\left(\frac{x_j - x_i}{j - i}\right) \forall i < j$, (11)where β indicates the trend magnitude of the data series, and x_i and x_j are the data values in the i-th and j-th years, respectively. An outcome where $\beta > 0$ ($\beta < 0$) represents a trend of increase (decrease).

The significance of the trend was examined further based on the nonparametric Mann–Kendall (MK) method (Mann, 1945; Kendall, 1975), which has been used widely for detection of the significance of trends in climatological and hydrological research (Liu et al., 2012; Soltani et al., 2012; Yue et al., 2018). The Z-statistic of the MK test follows the standard normal distribution with a mean value of 0 and standard deviation of 1. The null hypothesis means that there is no significant trend in the tested data series. An outcome where $|Z| > Z_{1-\alpha/2}$ indicates that the null hypothesis is rejected and the trend of the tested time series is significant at the confidence level of α. This study used set values of $\alpha = 0.05$ and $Z_{1-\alpha/2} = Z_{1-0.05/2} = 1.96$.

2.4. Computation of contribution of meteorological variables to drought

The flow diagram presented in Fig. 3 shows how the direct relative

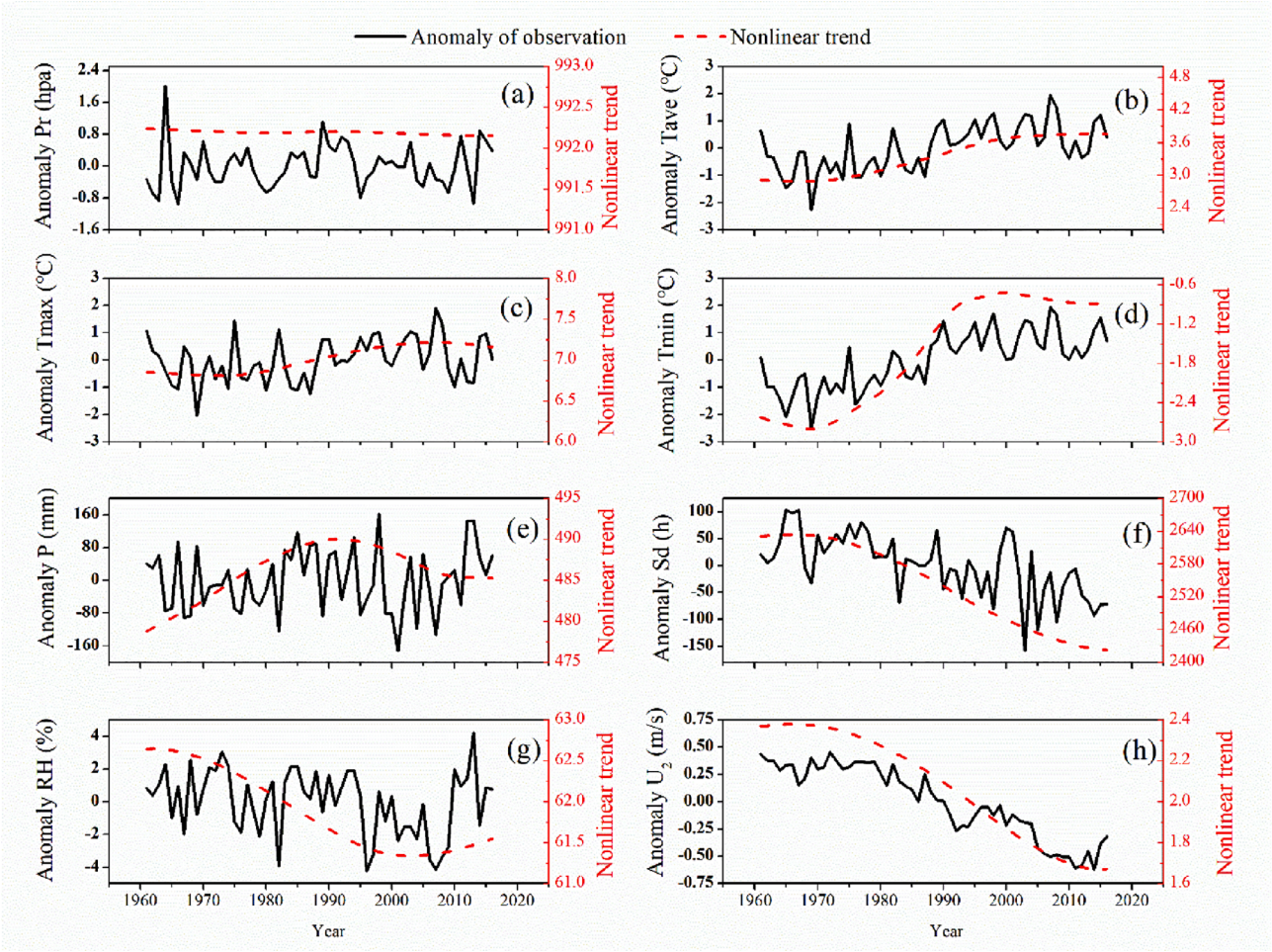

Fig. 4. Annual variations of the main climatic variables and their nonlinear trends extracted using the CEEMDAN method.

contributions of the meteorological variables to the drought trend in the SNP region were obtained.

First, the significance of the change of each meteorological variable was tested using the MK method.

Second, after finding the significantly changing variables, the CEEMDAN nonlinear detrending method was applied. In detail, the variable x series (i.e., daily temperature) from January 1, 1961 to December 31, 2016 was divided into 365 groups, as shown in the following square matrix $\begin{bmatrix} x_{1,1,1961} & x_{2,1,1961} & \cdots & x_{31,12,1961} \\ x_{1,1,1962} & x_{2,1,1962} & \cdots & x_{31,12,1962} \\ \vdots & \vdots & & \vdots \\ x_{1,1,2016} & x_{2,1,2016} & \cdots & x_{31,12,2016} \end{bmatrix}$, and the precipitation series from January 1961 to December 2016 was divided into 12 groups, as shown in the following square matrix $\begin{bmatrix} x_{1,1961} & x_{2,1961} & \cdots & x_{12,1961} \\ x_{1,1962} & x_{2,1962} & \cdots & x_{12,1962} \\ \vdots & \vdots & & \vdots \\ x_{1,2016} & x_{2,2016} & \cdots & x_{12,2016} \end{bmatrix}$. Each column in the matrix was considered a group, and the CEEMDAN method was used on each group to remove the nonlinear trend of the climatic variables.

Third, by combining the detrended data series and the observed data series as the input for the SPEI calculation, we obtained a series of numerical experiments that served as the basis for the primary analysis. In this regard, $SPEI_{OB\text{-}ALL}$ was the index calculated using all the observed meteorological variables, which referenced the full calculation, incorporating the changes in all the climatic variables. $SPEI_{DE\text{-}ALL}$, which was calculated using all the detrended meteorological variables, indicated the base drought condition if the climate change was not significant. $SPEI_i$ was calculated using the observed meteorological variable i and other detrended meteorological variables.

Finally, based on the above SPEI numerical experiments, the relative contributions of the significantly changing meteorological variables to the drought trend were distinguished. The trend slope of $SPEI_{DE\text{-}ALL}$ was defined as the baseline. Thus, the relative rate of change of the trend slopes of $SPEI_i$ to the trend of $SPEI_{DE\text{-}ALL}$ was regarded as the general contribution of meteorological variable i to the current drought trend in the SNP (expressed as Cr_i). The factors that affect drought consist not only of the significant climatic elements but also of other factors, e.g., human activities. Therefore, the relative rate of change of the trend slope of $SPEI_{OB\text{-}ALL}$ to the trend of $SPEI_{DE\text{-}ALL}$ could be regarded as the general contribution of all the different elements to the drought trend.

The relative rates of change were calculated as follows:

$$Cr_i = \frac{T_{SPEI_i} - T_{SPEI_{DE-ALL}}}{T_{SPEI_{DE-ALL}}} \times 100\%, \quad (12)$$

$$Cr_{other} = \frac{T_{SPEI_{OB-ALL}} - T_{SPEI_{DE-ALL}}}{T_{SPEI_{DE-ALL}}} \times 100\% - \left(\sum_{i=1}^{p} Cr_i\right), \quad (13)$$

where $T_{SPEI_{DE-ALL}}$, T_{SPEI_i}, and $T_{SPEI_{OB-ALL}}$ represent the trend slopes of the SPEI series in the different numerical experiments, and p denotes the number of significantly changing variables.

To understand and compare the relative magnitudes of the contributions of these variables to drought trend, the sum of the relative rates of change is expressed as 100 percentage. Hence, the relative contribution (Rc_i) of meteorological variable i to the drought tendency was calculated as follows:

$$Rc_i = \frac{Cr_i}{\sum_{i=1}^{p} Cr_i + Cr_{other}} \times 100\%, \quad (14)$$

Table 1
Results of the trend test on annual climatic variables in relation to the SNP.

	Pr(hpa)	Tave(℃)	Tmax(℃)	Tmin(℃)	P(mm)	Sd(h)	RH(%)	U_2(m/s)
β(unit/decade)	0.06	0.31	0.15	0.47	6.05	−23.12	−0.28	−0.19
Z	1.31	**4.47**	**2.06**	**5.84**	0.84	**−5.19**	−1.89	**−8.26**

Note: numbers in bold indicate a pass of the test at the 0.05 significance level.

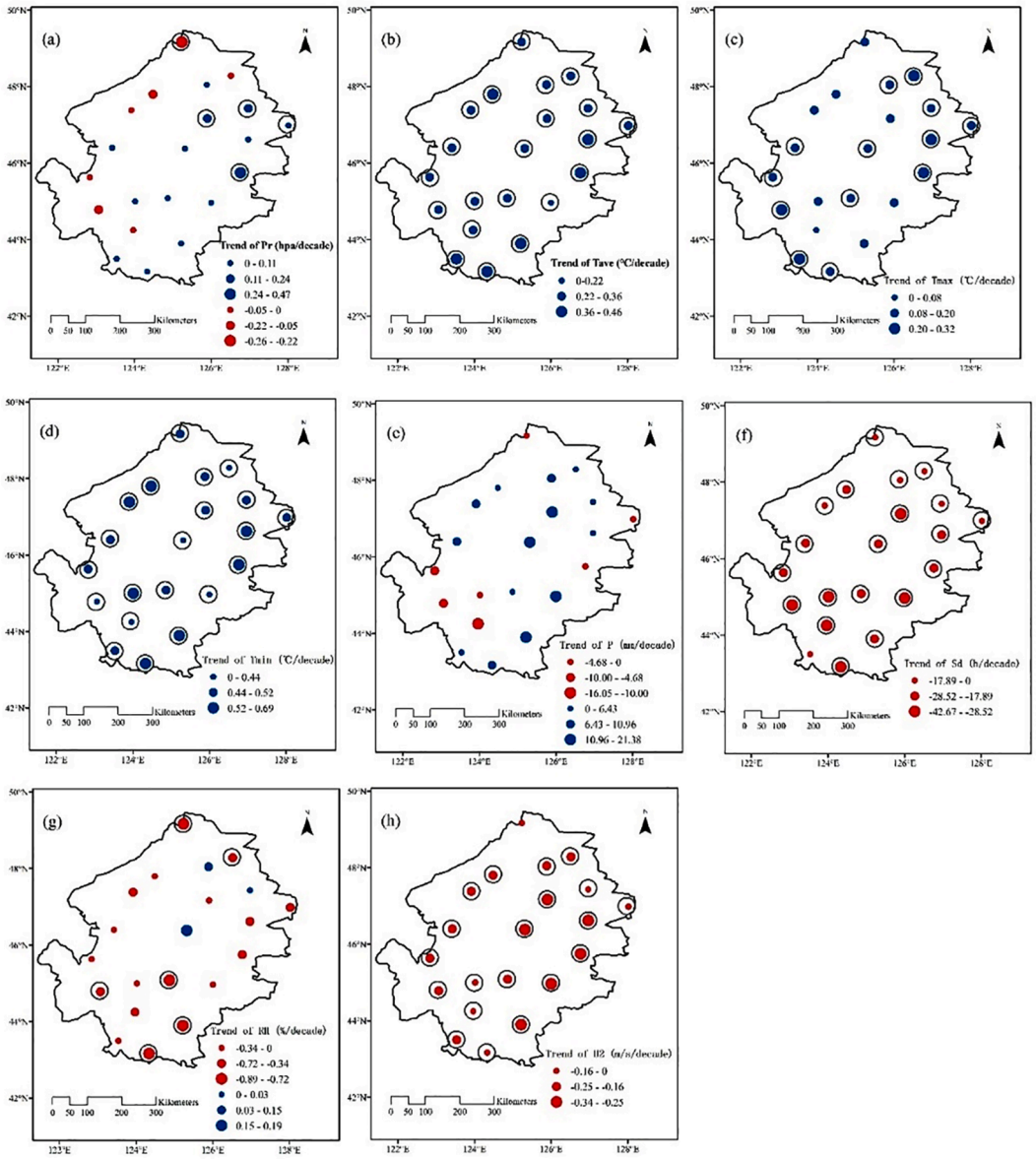

Fig. 5. Spatial distribution of climatic variable trends during 1961–2016: (a) Pr, (b) Tave, (c) Tmax, (d) Tmin, (e) P, (f) Sd, (g) RH, and (h) U_2 (for trends significant at the 0.05 significance level, a ring is placed around the solid dot).

3. Results

3.1. Spatiotemporal characteristics of climatic variables

The temporal change and nonlinear trend of eight meteorological variables during 1961–2016 are shown in Fig. 4. The residual series extracted using the CEEMDAN approach excludes the impact of the period of fluctuation and thus better expresses the nonlinear trend of each variable. It can be seen from Fig. 4 that a nonlinear trend of increase is evident for Tave, Tmax, and Tmin throughout the study period and before 1990 for P. Conversely, a trend of decrease is shown for Pr, Sd, RH, and U_2. Based on the MK results (Table 1), the meteorological variables of Tave, Tmax, Tmin, Sd, and U_2 have a significant trend of change on the SNP. The trend slopes of annual Tave, Tmax, and Tmin of 0.31, 0.15, and 0.47 ℃/10a, respectively, reflect that the increasing Tmin contributes most to the increase in average temperature on the SNP. Although P shows a trend of increase (rate: 6 mm/10a), the slope magnitude is not significant, which is consistent with the results of Faiz et al. (2018). The change point of the climatic variables in the SNP region is around 1990; subsequently, the values of annual Tave and Tmin are higher than the mean values, while the values of annual Sd, RH, and U_2 are lower than the mean values. It is worth noting that the climate of

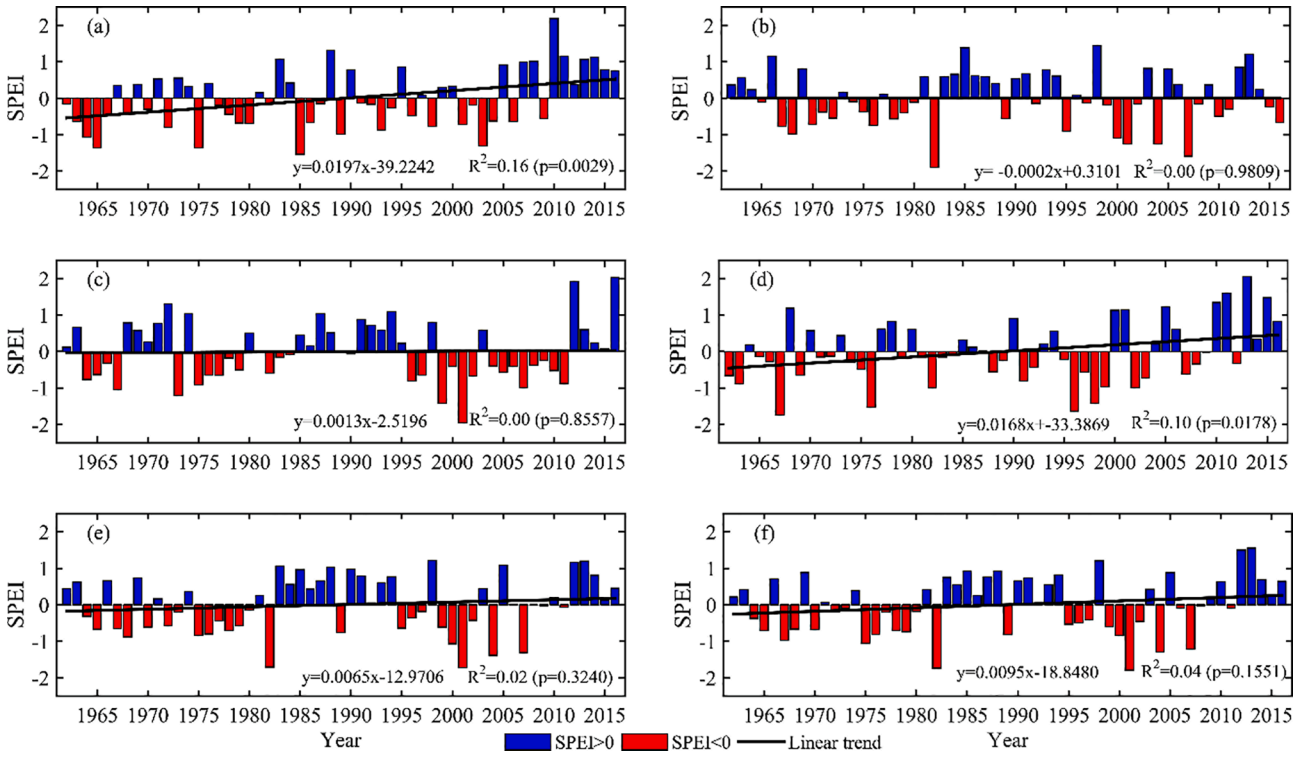

Fig. 6. Temporal change of the SPEI for the SNP at (a) spring, (b) summer, (c) autumn, (d) winter, (e) the growing season, and (f) annual timescales.

the SNP region has been highly impacted by the changing environment during 1961–2016.

The spatial distributions of the trends of the climatic variables in the SNP region are shown in Fig. 5. It can be seen that the SNP is dominated by increasing trends in Tave, Tmax, and Tmin (Fig. 5b–d) and decreasing trends in Sd, RH, and U_2 (Fig. 5f–h). Although the trend of precipitation is not significant, an increasing tendency can be observed at 14 of the 21 stations (Fig. 5e). The decreasing tendency of precipitation observed at the remaining seven stations, located mainly in the southwest of the SNP (Fig. 5e), is opposite to the trends seen for Pr and RH (Fig. 5a and 5g).

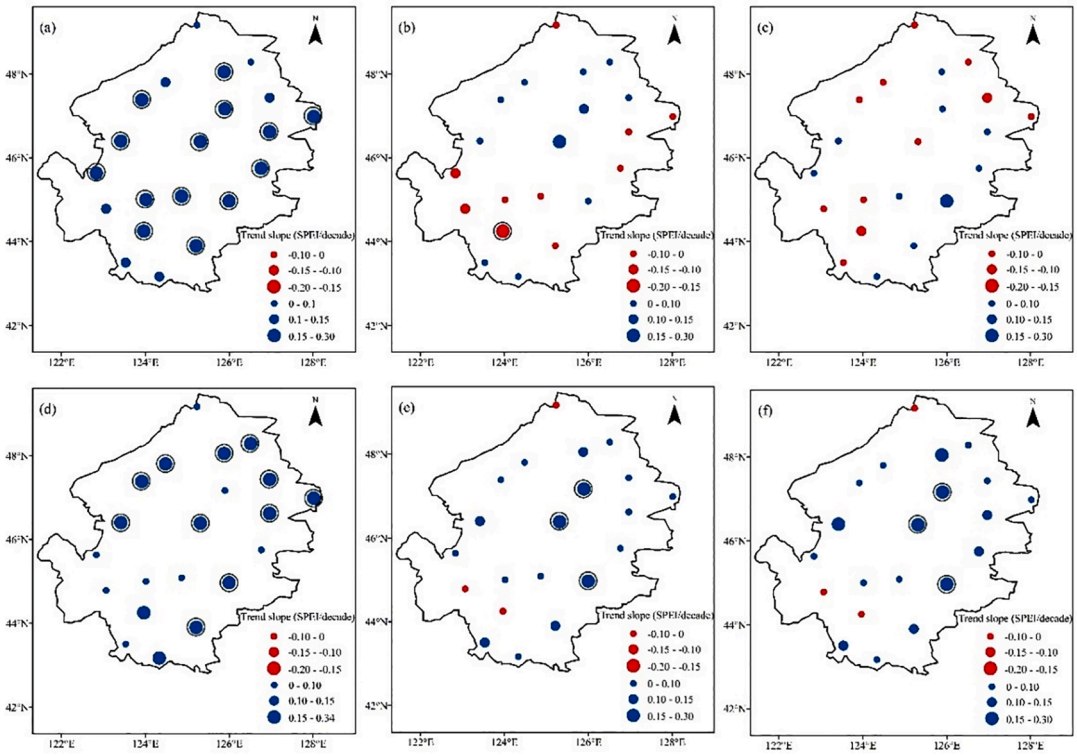

Fig. 7. Spatial distribution of the SPEI trend for the SNP at (a) spring, (b) summer, (c) autumn, (d) winter, (e) the growing season, and (f) annual timescales.

Overall, 14 (18) stations exhibit an increasing (decreasing) tendency for Pr (RH), and the area in which the increasing (decreasing) trend of Pr (RH) is significant is primarily in the east (south) of the SNP. Spatially, the climatic variables T (Tave, Tmax, Tmin), Sd, and U_2 show significant trends of change in the SNP region.

3.2. Spatiotemporal distribution of drought

3.2.1. Temporal trend

Average SPEI values on different timescales for the 21 stations on the SNP are displayed in Fig. 6. It can be seen that drought and wet periods occur alternately throughout 1962–2016. Overall, two principal periods of drought (1962–1982 and 1999–2007) and wetness (1983–1998 and 2010–2016) can be seen in the SNP region on the annual timescale and in the growing season. These evident periods with long duration of drought or wetness are also represented in summer and autumn; however, the trends of the SPEI in these two seasons are not as obvious (Fig. 6b and 6c). The alternating frequency of periods of drought and wet is higher in spring and winter, and more wet events are evident in the most recent five years, leading to an upward trend of the SPEI during the study period ($p < 0.05$, Fig. 6a and 6d). The frequency of drought on the SNP is largely the same as that of wet events, i.e., approximately 30%. However, it does show a slightly alleviated trend on the annual timescale (Fig. 6f), which is mainly influenced by the increasing trends of the SPEI in spring and winter, while the changes of the SPEI in summer and autumn are mainly responsible for the interannual variability of the drought and wet events.

3.2.2. Spatial pattern

The magnitude and significance of the SPEI trend during 1962–2016 at the seasonal, growing season, and annual timescales were detected using the MK method and are shown in Fig. 7. The spatial patterns of the SPEI trend in the SNP region vary with season. All 21 stations show an increasing tendency of the SPEI in spring and winter during the recent 55 years and 14 and 11 stations, respectively, present a significant trend of increase. In summer, 47.6% of the stations (mostly in the south) of the SNP region show a nonsignificant tendency of drought over the recent 55 years. Although 11 of the 21 stations show a nonsignificant trend of drying in autumn, the stations are scattered across the SNP and the trend is not as strong as in summer. Regionally, the absolute magnitude of the trend slope is higher in spring and winter (average: 0.19 and 0.17 /10a, respectively) than in summer and autumn (average: −0.006 and −0.007/10a, respectively). Annually and in the growing season, 18 of the 21 stations show an increasing trend of the SPEI, and the trend at the Mingshui, Anda, and Sanchahe stations is significant with a slope value of > 0.2 /10a. Nonsignificant drying trends are evident at the Tongyu, Changling, and Nenjiang stations, which are affected mainly by the drought tendency in summer and autumn. In addition, we compared the relationship between the modified soil water deficit index calculated in our previous study (Yang et al., 2017) and the SPEI in the growing season calculated in this study (Appendix Fig. A1). The SPEI shows positive correlation with the modified soil water deficit index at the Fuyu, Changling, Hailun, and Harbin stations for which the Spearman correlation coefficient r values reach 0.66 ($p < 0.01$), 0.69 ($p < 0.01$), 0.39 ($p < 0.01$), and 0.50 ($p < 0.01$), respectively, indicating that the SPEI could capture the deficit in soil moisture in the SNP region.

A significant distinct rise in temperature in the SNP region has been detected, and although greater evaporation might be expected under conditions of increasing temperature, the reverse trend has been observed in Northeast China, including the SNP region (Liu, 2004; Ma et al., 2017). It can be seen that the evolution of drought in the SNP region also depends on other factors, as indicated by the nonsignificant increases in the trends of annual precipitation (Table 1), consistent with the results of previous studies (Jia et al., 2019; Faiz et al., 2018; Ye et al., 2019). The variability of PET in Northeast China is higher than that of precipitation (Zhao et al., 2007). The fact that the nonsignificant increase in precipitation and decrease in evaporative demand (i.e., PET) might lead to mitigation of meteorological drought over the SNP (Fig. 7) is consistent with the results of Zhai et al. (2010), who indicated that the Songhua River Basin showed a marginally significant trend toward wetter conditions during 1961–2007.

Table 2
Description of the six different SPEI-based numerical experiments.

ID	Scenarios	Temperature (℃)	Precipitation (mm)	Net radiation (MJ/(m^2·d))	Wind speed(m/s)
1	$SPEI_{DE-ALL}$	Detrend	Detrend	Detrend	Detrend
2	$SPEI_T$	Observed	Detrend	Detrend	Detrend
3	$SPEI_P$	Detrend	Observed	Detrend	Detrend
4	$SPEI_R$	Detrend	Detrend	Observed	Detrend
5	$SPEI_U$	Detrend	Detrend	Detrend	Observed
6	$SPEI_{OB-ALL}$	Observed	Observed	Observed	Observed

3.3. Numerical experiment design

Although the change of precipitation in the SNP region is not significant, it is prerequisite for the occurrence of drought by any definition. Therefore, the contributions of T (Tmax, Tmin, and Tave), P, net radiation (R), and U_2 on the trend of drought were of primary concern in this study. By combining the detrended data series and observed data series as input for the SPEI calculation, we designed six different SPEI-based numerical experiments, as shown in Table 2.

The efficacy of separating the impacts of the changes of climatic variables on drought depends on these quantities being approximately independent in their contribution to the full hydroclimatic response ($SPEI_{OB-ALL}$). However, it is worth noting that the SPEI scenarios that retain a single observed variable while detrending the remainder actually cause disruption of the complex interactions underlying the meteorological variables. Nevertheless, these numerical experiments could represent an approach for synthetic analysis of one variable at a time. We compared $SPEI_{OB\_ALL}$ to the sum of $SPEI_P$, $SPEI_T$, $SPEI_R$, and $SPEI_U$ (expressed as $SPEI_{SUM}$) averaged over the entire study period for each station at different timescales. Considering the overlap of the detrended climatic variables in the sum of these four drought indices, we subtracted three times the base drought index ($SPEI_{DE-ALL}$) from the summed value. The relationship between $SPEI_{OB-ALL}$ and $SPEI_{SUM}$ is shown in Fig. 8. The 'SUM' and 'OB-ALL' values for each station track each other closely and are scattered evenly around the 1:1 line (the solid black line). This close match indicates that our SPEI-based numerical experiments are appropriate and acceptable, to a certain extent, for analysis of the influence of meteorological variables on drought trend in the SNP region.

The wet (1998) and drought (2001) years in Fig. 6f were selected as examples to discuss the differences between $SPEI_{DE-ALL}$ and $SPEI_{OB-ALL}$. As shown in the violin plots (Fig. 9), the SPEI performs well in capturing the wet and drought events on the SNP. For example, the average value of the annual SPEI ($SPEI_{DE-ALL}$ and $SPEI_{OB-ALL}$) for the 21 stations in 1998 is > 1, and wet periods occurred mainly in summer, autumn, and the growing season during this year (Fig. 9a), which is consistent with the description of flooding in 1998 in the Songhua River Basin (Song et al., 2015). In 2001, the average value of the annual SPEI is lower than − 1.5, and drought events occurred mainly in spring, summer, autumn, and the growing season (Fig. 9b). In comparison with the value of $SPEI_{DE-ALL}$, the average values of $SPEI_{OB-ALL}$ are higher in spring and winter (spring and the growing season) in 1998 (2001), indicating that climate change might have had minimal effect in mitigating drought conditions in the SNP region.

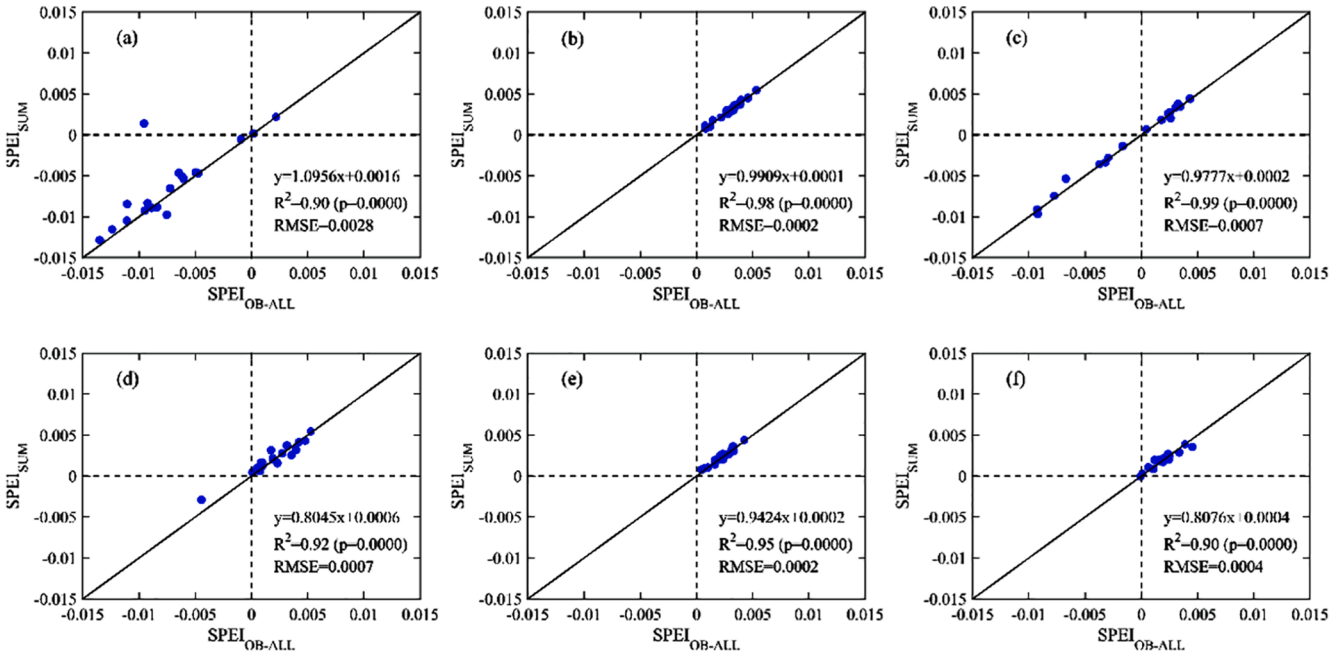

Fig. 8. Station comparisons between ensemble averaged $SPEI_{OB\text{-}ALL}$ and $SPEI_{SUM}$ at (a) spring, (b) summer, (c) autumn, (d) winter, (e) the growing season, and (f) annual timescales.

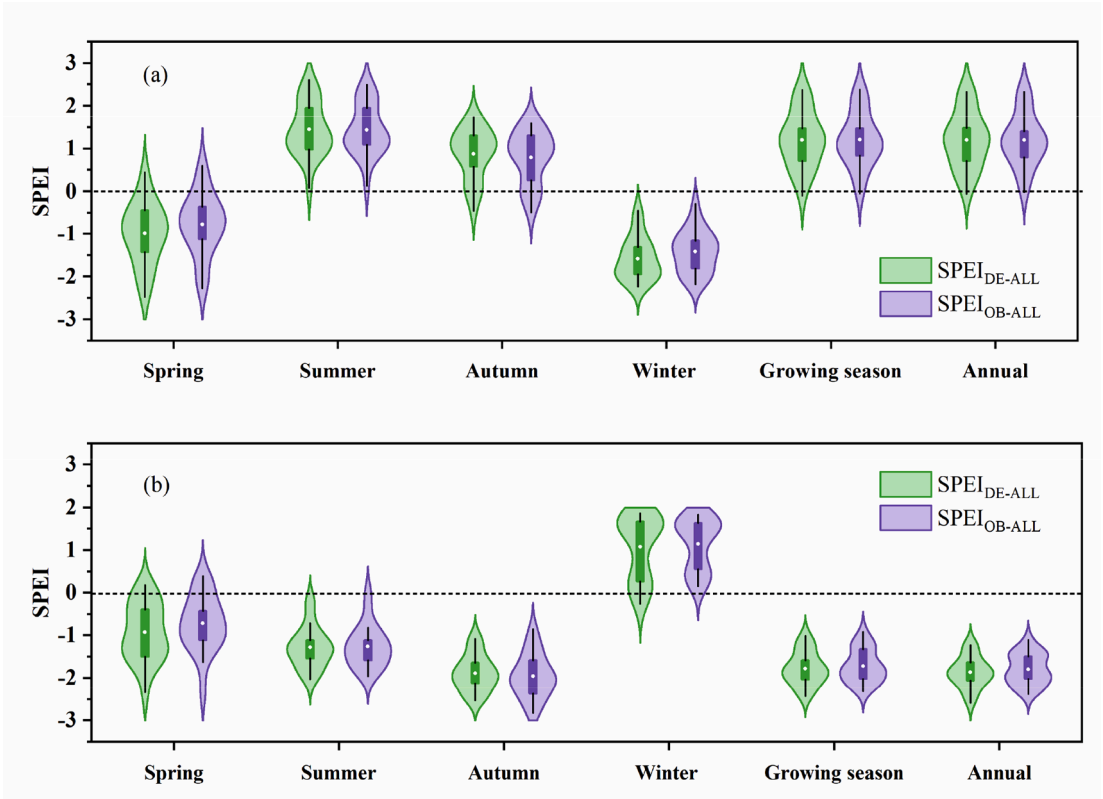

Fig. 9. Differences between $SPEI_{DE\text{-}ALL}$ and $SPEI_{OB\text{-}ALL}$ in (a) 1998 and (b) 2001.

3.4. Relative contributions of climatic variables to the current drought tendency

The relative contributions of P, T, R, and U_2 to the trend of drought on different timescales for the 21 stations on the SNP are shown in Fig. 10. If the relative contribution is negative, it means the change of this meteorological variable reduces the trend of the SPEI, indicating a tendency toward drought, and vice versa.

The perturbations of the climatic variables exhibit different roles in terms of modulating the drought trend in SNP. An increase in T results in a negative contribution to the trend of the SPEI. For example, regionally, the trend of the annual SPEI decrease by 9–31.8% owing to the obvious

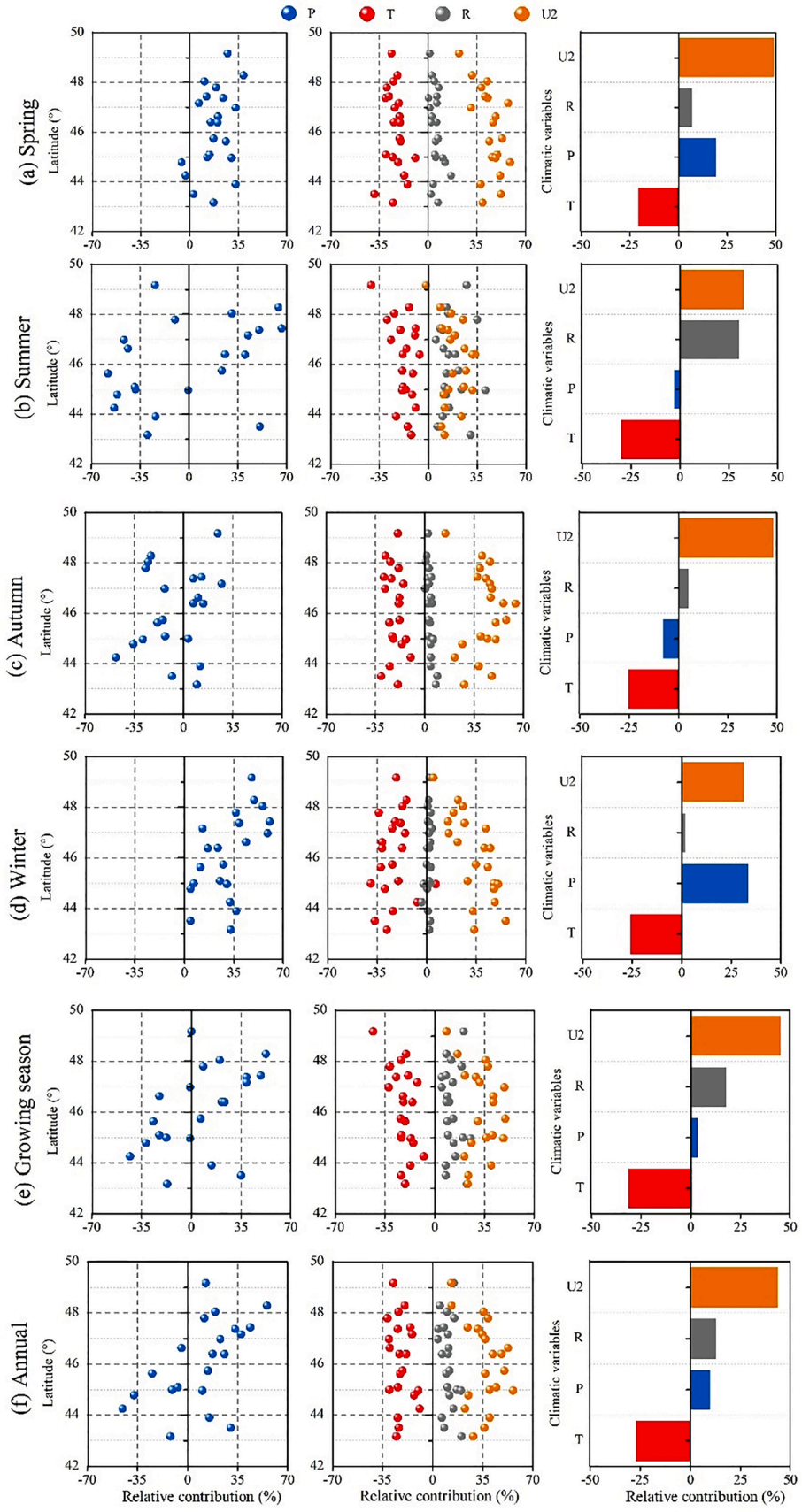

Fig. 10. Relative contributions of the nonlinear change of climatic variables to drought trend at (a) spring, (b) summer, (c) autumn, (d) winter, (e) the growing season, and (f) annual timescales.

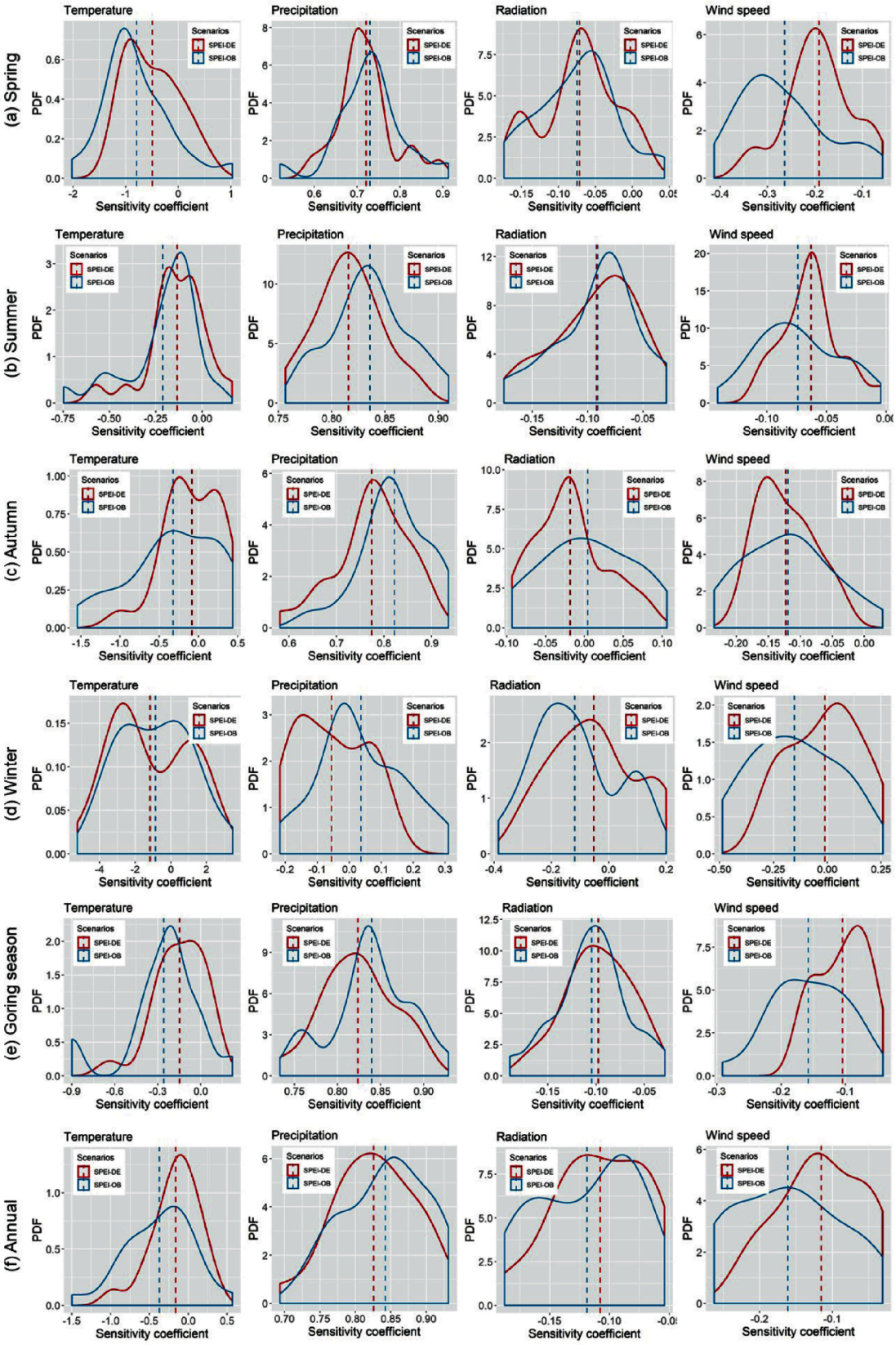

Fig. 11. The PDFs of the sensitivity coefficients of the climatic variables (with and without detrending) affecting drought over the SNP.

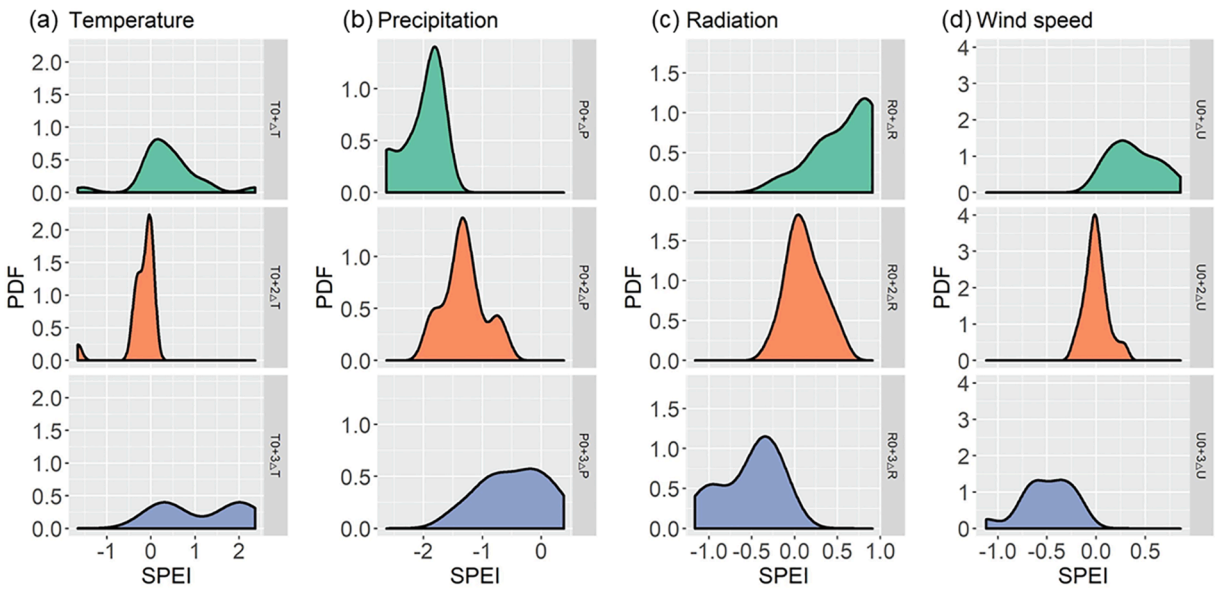

Fig. 12. The PDFs of the SPEI for different climatic variables at different gradients at the annual timescale.

increase in temperature, and the average contribution of the increase in T to the annual SPEI trend in the SNP region is − 27.8% (Fig. 10f). This characteristic is evident on other seasonal timescales, especially summer (Fig. 10b) and the growing season (Fig. 10e). Although an increase in temperature might lead to worse drought, the changes of drought characteristics in any particular area are the result of the combined effects of natural climatic variability. Significant decreasing trends of R and U_2 in the SNP region (Fig. 5) make a positive contribution to the SPEI trend. The average trend of the annual SPEI increases by 13.2% and 44% (Fig. 10f), respectively, owing to changes in R and U_2, which means that reductions in R and U_2 are primary factors forcing the SNP toward a slight wetter situation. The effects of these two elements on the trend of the SPEI differ seasonally and regionally. The contribution of U_2 to the alleviation of drought is larger in spring (49.2%, Fig. 10a), autumn (48.6%, Fig. 10c), and the growing season (45.6%, Fig. 10e) than in summer (32.8%, Fig. 10b) and winter (31.7%, Fig. 10d). Moreover, the high values are located in areas around 46°N (Fig. 10). The average contribution of R to the SPEI trend is highest in summer (30.6%, Fig. 10b), followed in descending order by that of the growing season (18.1%, Fig. 10e), spring (7.2%, Fig. 10a), autumn (5.2%, Fig. 10c), and winter (1.8%, Fig. 10d). Spatially, the directions of the change of the contributions from T, R, and U_2 to the SPEI trend for the 21 stations are consistent; however, this is not the case for the contribution from P. As the change of precipitation influenced by global warming remains uncertain, this leads to uncertainty regarding its contributions to the trend of drought in different regions and on different timescales. Regionally, the average trend of the annual SPEI in the SNP region is increased by 10.1% owing to the change of precipitation (Fig. 10f). This positive contribution is also detected in winter and spring, consistent with the results of Khan et al. (2016), who indicated that monthly precipitation in the Songhua River Basin is increased significantly in winter. However, the contribution of P change to the SPEI trend is negative in both summer and autumn, with the main contributing stations located in southern parts of the SNP, i.e., at latitudes below 46°N.

Overall, although increasing T in the SNP region would aggravate the drought condition, the decreasing U_2 would reduce the evaporative demand from the ground surface and mitigate the drying climatic conditions over the SNP. Therefore, the contributions of the changes in U_2 and R to the SPEI trend are the opposite to the contribution from T (Fig. 10), which is in agreement with the findings of previous study (Bertoldi et al., 2007; Zhang et al., 2016).

4. Discussion

4.1. Sensitivity of drought to climatic variables

The sensitivity of the SPEI drought index to the meteorological variables was analyzed based on standardized regression coefficients calculated using the "sensitivity" package in R. The greater the absolute value of the coefficient, the greater the influence of the corresponding variable on the change of the SPEI. For each station on the SNP, we calculated the sensitivity coefficients of the SPEI to the variables T, P, R, and U_2, both before and after detrending. The probability density functions (PDFs) of these sensitivity coefficients at different timescales are shown in Fig. 11.

It can be seen that both T and P show larger absolute values of the sensitivity coefficients in comparison with those of the other climatic variables, indicating that for the same degree change, T and P have larger effect on drought evolution over the SNP. On average, P has positive effect on the SPEI, whereas T, R, and U_2 have negative effects on the SPEI. However, from the spatial perspective, T, R, and U_2 have both negative and positive effects on the SPEI (Figs. S1-S6). This suggests that under the comprehensive influence of multiple variables, the effect of a single variable on drought is uncertain. For instance, P has positive effect on the SPEI in the SNP region in different seasons and on the annual timescale, indicating the crucial impact of precipitation on drought. Both R and U_2 have smaller negative effects on the SPEI during summer, the growing season, and on the annual timescale. Therefore, significant decreases in Sd and U_2 (Table 1) lead to an increase of the SPEI (Fig. 6). However, in spring (Fig. 11a and S1), autumn (Fig. 11c and S3), and winter (Fig. 11d and S4) positive effects of R and U_2 on the SPEI are detected at a few stations. For T, most stations show negative effects on drought at different timescales, although small positive effects are evident at a few stations (Figs. S1-S6).

By detrending the nonlinear trend of the meteorological variables, we found that the shapes of the PDFs of the sensitivity coefficients (red lines in Fig. 11) are changed. In comparison with the observed situation (blue lines in Fig. 11), the PDFs of the sensitivity coefficients of T, R, and U_2 are changed toward the right in most seasons, whereas the PDF of the sensitivity coefficient of precipitation is moved toward the left. This means that the sensitivity coefficients of the absolute values of drought to the detrended variables are mostly lower than to the observed variables, indicating that global climate change affects the sensitivity of drought to the climatic variables both temporally and spatially.

Table 3
Range of climatic variables over the SNP.

Timescale	Tave(℃)	P(mm)	R(MJ/m^2)	U_2(m/s)
Spring	0–16.5	0–276	690–966	0–5.7
Summer	17–27.5	80–735	877–1300	0–4
Autumn	−1–15	6–291	278–491	1–4.5
Winter	−26–1	0–55	5–200	0–5
Growing season	12–24	105–870	1600–2275	1–5
Annual	−2–16	120–960	1990–2885	1–4

4.2. Relationship between drought patterns and climatic variables

Taking the entire dataset together, the distribution of the SPEI is theoretically a normal distribution with a mean value of 0 and standard deviation of 1, which means that in a randomly changing climate system, the probability of drought (such as SPEI < 0) is relatively stable. However, this stability will be broken if a certain trend exists within the system, e.g., global climate change. The PDFs of the SPEI for the different variables in three gradients at different timescales are shown in Fig. 12 and S7–S11. Taking the annual timescale as an example, it can be seen that there is no overall decrease of the SPEI with an increase of the gradient $\triangle T = 6$ ℃ in average annual temperature. When T is increased from [T0, T0 + $\triangle$T) to the range of [T0 + $\triangle$T, T0 + 2$\triangle$T), the drought index shifts into the negative scope and the shape of the PDF becomes much sharper. However, when the temperature is increased from [T0, T0 + $\triangle$T) to [T0 + 2$\triangle$T, T0 + 3$\triangle$T), the drought index shifts toward the positive direction and the shape of PDF becomes flatter. This is most likely explained by interaction among the climatic variables. For example, previous research has indicated that water vapor would be increased by 6–7% globally if the temperature were to increase by 1 K (Held and Soden, 2006; Trenberth et al., 2014), while the rate of increase of precipitation would be almost 1–2%/K (Morice et al., 2012; O'Gorman et al., 2012). Wu and Chen (2019) also indicated that increasing temperature over the Pearl River Basin would not only increase the trends of drought duration and severity, but also enhance the trends of wetting duration and severity. Precipitation plays a decisive role in drought mitigation. It can be seen from Fig. 12b that when annual precipitation increases successively with a gradient of $\triangle P = 280$ mm, the PDF of the SPEI gradually moves toward the positive direction. As for R and U_2, there is consistent movement of the PDF of the SPEI in the negative direction with an increase in the gradient of $\triangle R = 295$ MJ/m^2 and $\triangle U_2 = 1$ m/s, respectively (Fig. 12c and 12d).

Seasonally, climatic variables differ widely in their range (Table 3) and therefore differences in the effects of the climatic variables on the PDFs of the SPEI are evident. With an increase of temperature, the SPEI generally decreases on seasonal timescales (Figs. S7–S11). An increase of spring P has considerable effect on drought relief over the SNP. The increase of net radiation at the seasonal scale makes the SPEI more concentrated, but the position of the PDF does not move substantially. Conversely, an increase in U_2 causes the position of the PDF to move in the negative direction during each of the four seasons and in the growing season.

Not only is there a gradual increase or decrease of the SPEI value with the changes of the climatic variables, but there is also a shift in the probability of whether drought conditions occur. It can be inferred that the distribution of drought results from dynamic interplay among the climatic variables on different timescales.

4.3. Other factors affecting drought

Drought is associated directly with water deficit and related indirectly to the atmospheric circulation and anthropogenic activities (Lin et al., 2018). For instance, Zhang et al. (2018b) indicated that when EI Niño strengthened, moisture conditions generally improved over the northern SNP, whereas La Niña events decreased the regional water availability. Li et al. (2015) highlighted that certain climate patterns (including the El Niño–Southern Oscillation, Atlantic Oscillation, Atlantic Multidecadal Oscillation, North Atlantic Oscillation, and Pacific Decadal Oscillation) have strong associations with precipitation observations. These teleconnection factors not only affect meteorological drought but they are also significantly associated with socioeconomic drought (Guo et al., 2019a). Anthropogenic activities can also have major influence on drought evolution. For example, with further increase in greenhouse gas emissions, surface net radiation will increase in most areas by inhibiting longwave cooling (Cook et al., 2014). Chen et al. (2011a) suggested that the effects of urbanization could affect the variation of temperature, precipitation, and relative humidity. Changes in sunshine duration, atmospheric aerosol concentrations, and land use/land cover can result in decreased surface solar radiation (Qian, 2016; Feng et al., 2019), which can lead to reduction of PET. Interaction between climate systems and human activities such as land greening and urbanization can contribute to the reduction of surface wind speed (Zhao et al., 2016; Zhang et al., 2019c), which can indirectly affect the dynamic factors associated with water evaporation.

4.4. Limitations

The contribution of each climatic variable to drought evolution was separated in this study by setting different numerical experiments using detrended variables. Although this is a recognized approach for synthetic analysis of one observed variable at a time, detrending does interfere with the complex correlation among climatic variables. General circulation models can simulate various climatic variables in different scenarios under the premise of considering the interaction between the land surface, atmosphere, ocean, and other modules. Therefore, future research could focus on using simulation data to analyze the contributions of different factors to drought evolution on larger spatial scale.

5. Conclusions

The spatial and temporal characteristics of the trend of drought at 21 stations distributed across the SNP were analyzed on different timescales using site observations acquired during the previous five decades. Results suggest that annual drought over the SNP has presented a trend of mitigation with three of the stations showing a significant increasing trend of the SPEI at the 0.05 confidence level. All stations had positive trends of the SPEI in spring and winter with the trend at 14 and 11 stations, respectively, significant at the 0.05 confidence level. However, the trends of the SPEI were inconsistent spatially over the SNP in summer and autumn. Generally, it is likely that the SNP experienced wetting and warming climatic conditions during 1961–2016.

To investigate the relative contributions of different climatic variables with significant change to the drought mitigation tendency, we designed a series of SPEI-based numerical experiments: a baseline case without significant climate change, a current case with all observed data, and four separate cases that maintained the individual trend in one meteorological variable. Temperature over the SNP was found to have increased significantly, and the rate of change of increase aggravated the drought tendency at all timescales, i.e., the contribution was − 21.2%, −30.6%, −25.6%, −26.2%, −31.7%, and − 27.8% in spring, summer, autumn, winter, the growing season, and on the annual timescale, respectively. However, with the comprehensive impacts of other climatic variables, the drought condition of the SNP was mitigated slightly in comparison with the numerical experiment in which all four climatic variables (T, P, R, U_2) were free of nonlinear trends. Comparatively, the contribution of the decreasing trend in U_2 to the positive trend of the SPEI was larger than that of net radiation, i.e., 7.2%, 30.6%, 5.2%, 1.8%, 18.1%, and 13.2% for R and 49.2%, 32.8%, 48.6%, 31.7%, 45.6%, and 44.0% for U_2 in spring, summer, autumn, winter, the growing season, and on the annual timescale, respectively. The dominant effect of the

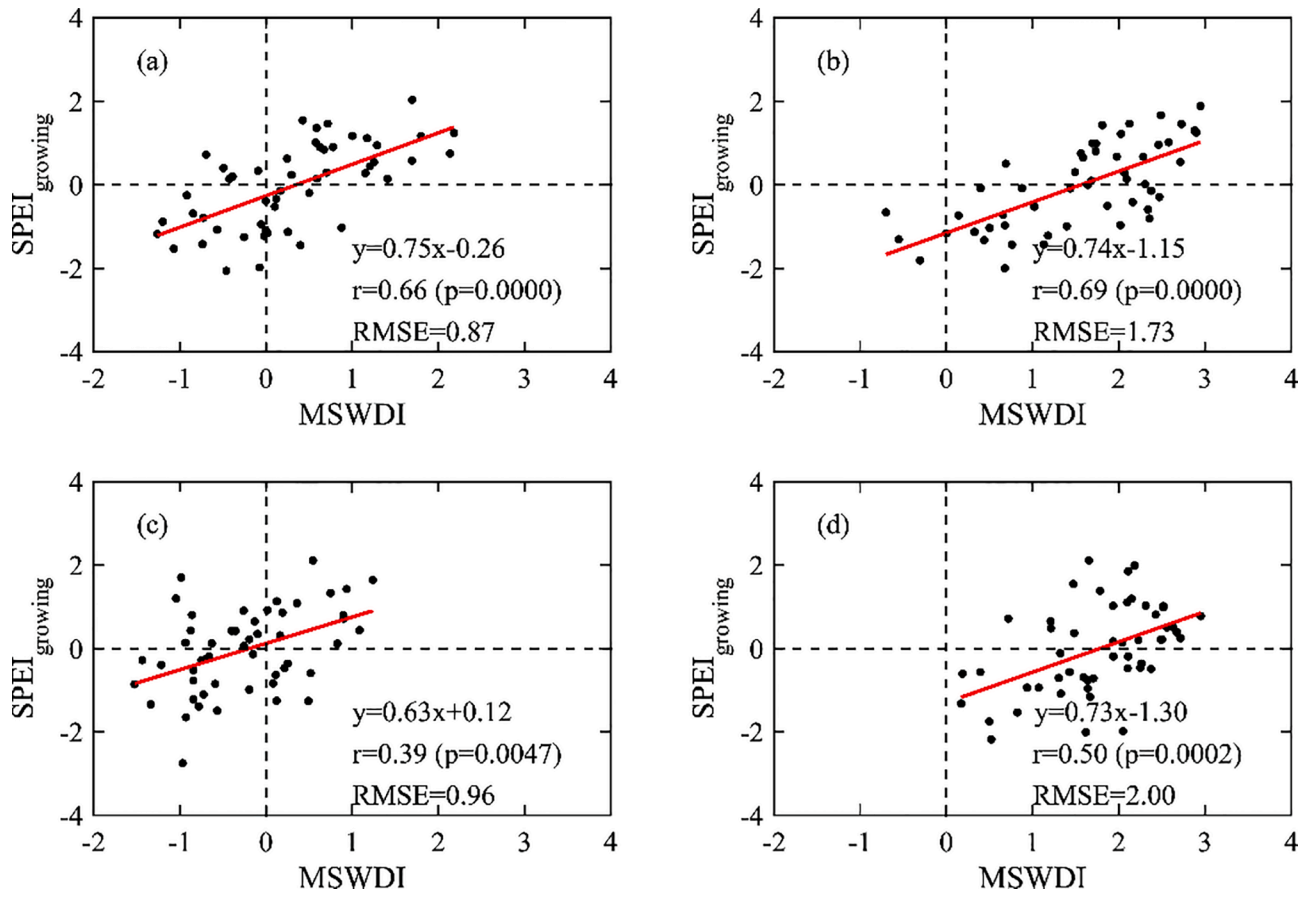

Fig. A1. Correlation between the modified soil water deficit index (MSWDI) calculated in our previous study and SPEI at growing season calculated in this study at (a) Fuyu, (b) Changling, (c) Hailun, and (d) Harbin stations.

change in precipitation on the SPEI trend varied with season and region. In summer and autumn, the trend of precipitation led to a decrease in the SPEI trend of 3.3% and 8.3%, respectively, which was concentrated in areas of the SNP south of 46°N. In spring and winter, the SPEI trend at almost all stations was increased by 19.5% and 33.9%, respectively, indicating that the change of P in winter and spring plays a major role in driving the mitigation of annual drought in the SNP region.

CRediT authorship contribution statement

Ruxin Zhao: Methodology, Writing - original draft, Writing - review & editing, Formal analysis. **Huixiao Wang:** Conceptualization, Funding acquisition. **Ji Chen:** Writing - review & editing, Conceptualization. **Guobin Fu:** Software, Validation. **Chesheng Zhan:** Supervision, Resources. **Huicai Yang:** Methodology, Software, Validation.

Declaration of Competing Interest

The authors declare that they have no known competing financial interests or personal relationships that could have appeared to influence the work reported in this paper.

Acknowledgement

We gratefully acknowledge the China Meteorological Administration for providing the climate datasets.

Funding

This work was supported by the National Key Research and Development Program of China (Grant No. 2017YFC0404603) and National Natural Science Foundation of China (Grant No. 51779009), 111 Project (B18006).

Appendix

(Fig. A1)

Appendix A. Supplementary data

Supplementary data to this article can be found online at https://doi.org/10.1016/j.ecolind.2020.107107.

References

Abramowitz, M., Stegun, I.A., 1965. Handbook of Mathematical Functions. Dover Publications, New York.

Allan, R.P., Soden, B.J., 2008. Atmospheric Warming and the Amplification of Precipitation Extremes. Science 321 (5895), 1481–1484.

Allen, R.G., et al., 1998. Crop Evapotranspiration: Guidelines for Computing Crop Requirements FAO Irrigation and Drainage Paper, No. 56. FAO, Rome, Italy.

Beguería, S., Vicente-Serrano, S.M., Reig, F., Latorre, B., 2014. Standardized precipitation evapotranspiration index (SPEI) revisited: parameter fitting, evapotranspiration models, tools, datasets and drought monitoring. Int. J. Climatol. 34 (10), 3001–3023.

Bertoldi, G., Albertson, J.D., Kustas, W.P., Li, F., Anderson, M.C., 2007. On the opposing roles of air temperature and wind speed variability in flux estimation from remotely sensed land surface states. Water Resour. Res. 43 (10) https://doi.org/10.1029/2007WR005911.

Carrão, H., Naumann, G., Barbosa, P., 2018. Global projections of drought hazard in a warming climate: a prime for disaster risk management. Clim Dyn 50 (5-6), 2137–2155.

Chen, J., Li, Q., Niu, J., Sun, L., 2011. Regional climate change and local urbanization effects on weather variables in Southeast China. Stoch Environ Res Risk Assess 25 (4), 555–565.

Chen, H., Sun, J., 2017. Anthropogenic warming has caused hot droughts more frequently in China. Journal of Hydrology 544, 306–318.
Chen, Z., Wei, W., Liu, J., Wang, Y., Chen, J., 2011b. Identifying the recharge sources and age of groundwater in the Songnen Plain (Northeast China) using environmental isotopes. Hydrogeol. J. 19 (1), 163–176.
Colominas, M.A., Schlotthauer, G., Torres, M.E., 2014. Improved complete ensemble EMD: A suitable tool for biomedical signal processing. Biomed. Sign. Process. Control 14, 19–29.
Cook, B.I., Smerdon, J.E., Seager, R., Coats, S., 2014. Global warming and 21st century drying. Clim. Dyn. 43 (9-10), 2607–2627.
Dai, A., 2011. Drought under global warming: a review: Drought under global warming. WIREs Clim Change 2 (1), 45–65.
Dai, A., 2013. Increasing drought under global warming in observations and models. Nature Clim Change 3 (1), 52–58.
Donohue, R.J., McVicar, T.R., Roderick, M.L., 2010. Assessing the ability of potential evaporation formulations to capture the dynamics in evaporative demand within a changing climate. J. Hydrol. 386 (1-4), 186–197.
Easterling, D.R., Wallis, T.W.R., Lawrimore, J.H., Heim Jr., R.R., 2007. Effects of temperature and precipitation trends on U.S. drought. Geophys. Res. Lett. 34 (20) https://doi.org/10.1029/2007GL031541.
Faiz, M.A., Liu, D., Fu, Q., Sun, Q., Li, M.o., Baig, F., Li, T., Cui, S., 2018. How accurate are the performances of gridded precipitation data products over Northeast China? Atmosph. Res. 211, 12–20.
Feng, Y., Chen, D., Zhao, X., 2019. Estimated long-term variability of direct and diffuse solar radiation in North China during 1959–2016. Theor Appl Climatol 137 (1-2), 153–163.
Giorgi, F., et al., 2019. The response of precipitation characteristics to global warming from climate projections. Earth System Dynamics 10(1), 73-89. Doi: 10.5194/esd-10-73-2019.
Guo, Y.i., Huang, S., Huang, Q., Wang, H., Wang, L.u., Fang, W., 2019a. Copulas-based bivariate socioeconomic drought dynamic risk assessment in a changing environment. J. Hydrol. 575, 1052–1064.
Guo, E., Zhang, J., Wang, Y., Quan, L., Zhang, R., Zhang, F., Zhou, M.o., 2019b. Spatiotemporal variations of extreme climate events in Northeast China during 1960–2014. Ecol. Indicat. 96, 669–683.
Guzman-Morales, J., Gershunov, A., 2019. Climate Change Suppresses Santa Ana Winds of Southern California and Sharpens Their Seasonality. Geophys. Res. Lett. 46 (5), 2772–2780. https://doi.org/10.1029/2018gl080261.
Hamon, W.R., 1961. Estimating potential evapotranspiration. Proc. Amer. Soc. Civ. Engrs. 87, 107–120.
Heim Jr., R.R., 2002. A Review of Twentieth-Century Drought Indices Used in the United States. Bull. Amer. Meteor. Soc. 83 (8), 1149–1166.
Held, I.M., Soden, B.J., 2006. Robust responses of the hydrological cycle to global warming. J Climate. 19, 5686-5699.
Hsiang, S.M., et al., 2013. Quantifying the influence of climate on human conflict. Science 341, 1212. DOI: 10.1126/science.1235367#comments.
Huang, N.E., Shen, Z., Long, S.R., Wu, M.C., Shih, H.H., Zheng, Q., Yen, N.-C., Tung, C.C., Liu, H.H., 1998. The empirical mode decomposition and the Hilbert spectrum for nonlinear and non-stationary time series analysis. Proc. R. Soc. Lond. A 454 (1971), 903–995.
Huntington, T.G., 2006. Evidence for intensification of the global water cycle: Review and synthesis. J. Hydrol. 319 (1-4), 83–95.
Irmak, S., Kabenge, I., Skaggs, K.E., Mutiibwa, D., 2012. Trend and magnitude of changes in climate variables and reference evapotranspiration over 116-yr period in the Platte River Basin, central Nebraska–USA. J. Hydrol. 420-421, 228–244.
Jeong, D.I., Sushama, L., Naveed Khaliq, M., 2014. The role of temperature in drought projections over North America. Climatic Change 127 (2), 289–303.
Jhajharia, D., Dinpashoh, Y., Kahya, E., Singh, V.P., Fakheri-Fard, A., 2012. Trends in reference evapotranspiration in the humid region of northeast India. Hydrol. Process. 26 (3), 421–435.
Jia, H., et al., 2019. Impact of Climate Change on the Water Requirements of Oat in Northeast and North China. WATER 11, 91. DOI:10.3390/w11010091.
Jiang, P., et al., 2018. Physiological and Dry Matter Characteristics of Spring Maize in Northeast China under Drought Stress. Water 10, 1561. DOI: 10.3390/w10111561.
Jiang, S., Liang, C., Cui, N., Zhao, L.u., Du, T., Hu, X., Feng, Y.u., Guan, J., Feng, Y.i., 2019. Impacts of climatic variables on reference evapotranspiration during growing season in Southwest China. Agricult. Water Manage. 216, 365–378.
Kang, L., Zhang, H., 2016. A Comprehensive Study of Agricultural Drought Resistance and Background Drought Levels in Five Main Grain-Producing Regions of China. Sustainability 8, 346. DOI: 10.3390/su8040346.
Kendall, M.G., 1975. Rank auto-correlation methods. Charles Griffin, London.
Khan, M.I., Liu, D., Fu, Q., Dong, S., Liaqat, U.W., Faiz, M.A., Hu, Y., Saddique, Q., 2016. Recent Climate Trends and Drought Behavioral Assessment Based on Precipitation and Temperature Data Series in the Songhua River Basin of China. Water Resour. Manage. 30 (13), 4839–4859.
Leng, G., Tang, Q., Rayburg, S., 2015. Climate change impacts on meteorological, agricultural and hydrological droughts in China. Global Planet. Change 126, 23–34.
Li, Y.i., Sun, C., 2017. Impacts of the superimposed climate trends on droughts over 1961–2013 in Xinjiang, China. Theor. Appl. Climatol. 129 (3-4), 977–994.
Li, C., Wu, P.T., Li, X.L., Zhou, T.W., Sun, S.K., Wang, Y.B., Luan, X.B., Yu, X., 2017. Spatial and temporal evolution of climatic factors and its impacts on potential evapotranspiration in Loess Plateau of Northern Shaanxi, China. Sci. Total Environ. 589, 165–172.
Li, J.Z., Wang, Y.X., Li, S.F., Hu, R., 2015. A Nonstationary Standardized Precipitation Index incorporating climate indices as covariates. J. Geophys. Res. Atmos. 120 (23) https://doi.org/10.1002/jgrd.v120.2310.1002/2015JD023920.
Li, X., Li, Y., Chen, A., Gao, M., Slette, I.J., Piao, S., 2019. The impact of the 2009/2010 drought on vegetation growth and terrestrial carbon balance in Southwest China. Agricult. Forest Meteorol. 269-270, 239–248.
Liang, L., Li, L., Liu, Q., 2011. Spatio-temporal variations of reference crop evapotranspiration and pan evaporation in the West Songnen Plain of China. Hydrol. Sci. J. 56 (7), 1300–1313.
Lin, L., Gettelman, A., Fu, Q., Xu, Y., 2018. Simulated differences in 21st century aridity due to different scenarios of greenhouse gases and aerosols. Climatic Change 146 (3-4), 407–422.
Liu, B., 2004. A spatial analysis of pan evaporation trends in China, 1955–2000. J. Geophys. Res. 109 (D15) https://doi.org/10.1029/2004JD004511.
Liu, F., Chen, S., Dong, P., Peng, J., 2012. Spatial and temporal variability of water discharge in the Yellow River Basin over the past 60 years. J. Geogr. Sci. 22 (6), 1013–1033.
Liu, X., Pan, Y., Zhu, X., Yang, T., Bai, J., Sun, Z., 2018. Drought evolution and its impact on the crop yield in the North China Plain. J. Hydrol. 564, 984–996.
Lobell, D.B., Schlenker, W., Costa-Roberts, J., 2011. Climate Trends and Global Crop Production Since 1980. Science 333 (6042), 616–620.
Ma, Q., et al., 2017. Changes of Reference Evapotranspiration and Its Relationship to Dry/Wet Conditions Based on the Aridity Index in the Songnen Grassland, Northeast China. WATER 9, 316. DOI: 10.3390/w9050316.
Mann, H.B., 1945. Nonparametric Tests Against Trend. Econometrica 13 (3), 245. https://doi.org/10.2307/1907187.
May, W., Rummukainen, M., Chéruy, F., Hagemann, S., Meier, A., 2017. Contributions of soil moisture interactions to future precipitation changes in the GLACE-CMIP5 experiment. Clim. Dyn. 49 (5-6), 1681–1704.
McKee, T.B., et al., 1993. The relationship of drought frequency and duration to time scales. In: Proceedings of the 8th Conference on Applied Climatology. Boston, MA: American Meteorological Society 17(22), 179-183.
Meng, X., et al., 2019. Long-Term Spatiotemporal Variations in Soil Moisture in North East China Based on 1-km Resolution Downscaled Passive Microwave Soil Moisture Products. Sensors 19(16), 3527. https://doi.org/10.3390/s19163527.
Mishra, A.K., Singh, V.P., 2010. A review of drought concepts. J. Hydrol. 391 (1-2), 202–216.
Morice, C.P., Kennedy, J.J., Rayner, N.A., Jones, P.D., 2012. Quantifying uncertainties in global and regional temperature change using an ensemble of observational estimates: The HadCRUT4 data set. J. Geophys. Res. 117 (D8), n/a–n/a.
Nguvava, M., Abiodun, B.J., Otieno, F., 2019. Projecting drought characteristics over East African basins at specific global warming levels. Atmosph. Res. 228, 41–54.
O'Gorman, P.A., Allan, R.P., Byrne, M.P., Previdi, M., 2012. Energetic Constraints on Precipitation Under Climate Change. Surv. Geophys. 33 (3-4), 585–608.
Ozdogan, M., Salvucci, G.D., 2004. Irrigation-induced changes in potential evapotranspiration in southeastern Turkey: test and application of Bouchet's complementary hypothesis. Water Resour. Res. 40 (4), W04301. https://doi.org/10.1029/2003WR002822.
Pachauri, R.K., et al., 2014. Climate Change 2014: Synthesis Report. Contribution of Working Groups I, II and III to the Fifth Assessment Report of the Intergovernmental Panel on Climate Change.
Papalexiou, S.M., Montanari, A., 2019. Global and Regional Increase of Precipitation Extremes under Global Warming. Water Resour. Res. 55 (6), 4901–4914. https://doi.org/10.1029/2018WR024067.
Pereira, L.S., Allen, R.G., Smith, M., Raes, D., 2015. Crop evapotranspiration estimation with FAO56: Past and future. Agricult. Water Manage. 147, 4–20.
Priestley, C.H.B., Taylor, R.J., 1972. On the assessment of surface heat flux and evaporation using large-scale parameters. Mon. Wea Rev. 100, 81–92. https://doi.org/10.1175/1520-0493(1972)100<0081:OTAOSH>2.3.CO;2.
Qian, C., 2016. Impact of land use/land cover change on changes in surface solar radiation in eastern China since the reform and opening up. Theor. Appl. Climatol. 123 (1-2), 131–139.
Samaniego, L., Thober, S., Kumar, R., Wanders, N., Rakovec, O., Pan, M., Zink, M., Sheffield, J., Wood, E.F., Marx, A., 2018. Anthropogenic warming exacerbates European soil moisture droughts. Nature Clim Change 8 (5), 421–426.
Sen, P.K., 1968. Estimates of the regression coefficient based on Kendall's tau. J. Am. Stat. Assoc. 63 (324), 1379–1389. https://doi.org/10.2307/2285891.
Soltani, S., Saboohi, R., Yaghmaei, L., 2012. Rainfall and rainy days trend in Iran. Climatic Change 110 (1-2), 187–213.
Song, X., Song, S., Sun, W., Mu, X., Wang, S., Li, J., Li, Y.i., 2015. Recent changes in extreme precipitation and drought over the Songhua River Basin, China, during 1960–2013. Atmosph. Res. 157, 137–152.
Song, X., Li, L., Fu, G., Li, J., Zhang, A., Liu, W., Zhang, K., 2014. Spatial–temporal variations of spring drought based on spring-composite index values for the Songnen Plain, Northeast China. Theor. Appl. Climatol. 116 (3-4), 371–384.
Sun, C., Ma, Y., 2015. Effects of non-linear temperature and precipitation trends on Loess Plateau droughts. Quat. Int. 372, 175–179.
Sun, S., Chen, H., Ju, W., Wang, G., Sun, G.e., Huang, J., Ma, H., Gao, C., Hua, W., Yan, G., 2017. On the coupling between precipitation and potential evapotranspiration: contributions to decadal drought anomalies in the Southwest China. Clim. Dyn. 48 (11-12), 3779–3797.
Tang, K.H.D., 2019. Climate change in Malaysia: Trends, contributors, impacts, mitigation and adaptations. Sci. Total Environ. 650, 1858–1871.
Teuling, A.J., 2018. A hot future for European droughts. Nat. Clim. Change 8 (5), 364–365.
Trenberth, K.E., et al., 2014. Seasonal aspects of the recent pause in surface warming. Nat. Clim. Change. 4, 911–916. https://doi.org/10.1038/nclimate2341.
Trenberth, K.E., 2011. Changes in precipitation with climate change. Clim. Res. 47 (1), 123–138.

Vicente-Serrano, S.M., et al., 2010. A multiscalar drought index sensitive to global warming: the standardized precipitation evapotranspiration index. J. Clim. 23 (7), 1696-1718. https://doi.10.1175/2009JCLI2909.1.

Wang, H., et al., 2015. Commonly Used Drought Indices as Indicators of Soil Moisture in China. J. Hydrometeorol. 16, 1397-1408. DOI: 10.1175/JHM-D-14-0076.1.

Wang, Q., Wu, J., Lei, T., He, B., Wu, Z., Liu, M., Mo, X., Geng, G., Li, X., Zhou, H., Liu, D., 2014. Temporal-spatial characteristics of severe drought events and their impact on agriculture on a global scale. Quaternary International 349, 10–21.

Wells, N., et al., 2004. A self-calibrating palmer drought severity index. J. Clim. 17, 2335–2351. https://doi.org/10.1175/1520-0442(2004)017<2335:ASPDSI>2.0.CO;2.

Williams, A.P., Seager, R., Abatzoglou, J.T., Cook, B.I., Smerdon, J.E., Cook, E.R., 2015. Contribution of anthropogenic warming to California drought during 2012–2014. Geophys. Res. Lett. 42 (16), 6819–6828.

WMO. 2006. Drought monitoring and early warning: Concepts, progress and future challenges. WMO-No. 1006, World Meteorological Organization, Geneva, Switzerland.

Wu, J., Chen, X., 2019. Spatiotemporal trends of dryness/wetness duration and severity: The respective contribution of precipitation and temperature. Atmosph. Res. 216, 176–185.

Wu, Z.H., et al., 2009. The multi-dimensional ensemble empirical mode decomposition method. Adv. Adapt. Data Anal. 1 (3), 339-372. DOI: 10.1142/s1793536909000187.

Xia, L., et al., 2018. SPI-Based Analyses of Drought Changes over the Past 60 Years in China's Major Crop-Growing Areas. Remote Sens-Basel 10, 171. DOI: 10.3390/rs10020171.

Yang, H., Wang, H., Fu, G., Yan, H., Zhao, P., Ma, M., 2017. A modified soil water deficit index (MSWDI) for agricultural drought monitoring: Case study of Songnen Plain, China. Agricult. Water Manage. 194, 125–138.

Ye, L., et al., 2019. Spatio-Temporal Analysis of Drought Indicated by SPEI over Northeastern China. WATER 11, 908. https://doi.org/10.3390/w11050908.

Yin, YunHe, Wu, ShaoHong, Dai, ErFu, 2010. Determining factors in potential evapotranspiration changes over China in the period 1971–2008. Chin. Sci. Bull. 55 (29), 3329–3337.

Yue ,Y., et al., 2018. Trend and Variability in Droughts in Northeast China Based on the Reconnaissance Drought Index. WATER 10, 318. DOI: 10.3390/w10030318.

Zhai, J.Q., Liu, B.o., Hartmann, H., Da Su, B.u., Jiang, T., Fraedrich, K., 2010. Dryness/wetness variations in ten large river basins of China during the first 50 years of the 21st century. Quat. Int. 226 (1-2), 101–111.

Zhang, J., Shen, Y., 2019. Spatio-temporal variations in extreme drought in China during 1961–2015. J. Geogr. Sci. 29 (1), 67–83.

Zhang, J., Sun, F., Xu, J., Chen, Y., Sang, Y.-F., Liu, C., 2016. Dependence of trends in and sensitivity of drought over China (1961–2013) on potential evaporation model. Geophys. Res. Lett. 43 (1), 206–213.

Zhang, L., Wang, C., Li, X., Zhang, H., Li, W., Jiang, L., 2018a. Impacts of agricultural expansion (1910s–2010s) on the water cycle in the songneng plain, Northeast China. Remote Sens. 10, 1108. http://www.mdpi.com/2072-4292/10/7/1108.

Zhang, X., Liu, X., Wang, W., Zhang, T., Zeng, X., Xu, G., Wu, G., Kang, H., 2018b. Spatiotemporal variability of drought in the northern part of northeast China. Hydrol. Processes 32 (10), 1449–1460.

Zhang, Y., Li, G., Ge, J., Li, Y., Yu, Z., Niu, H., 2019b. sc_PDSI is more sensitive to precipitation than to reference evapotranspiration in China during the time period 1951–2015. Ecol. Indicat. 96, 448–457.

Zhang, Z., et al., 2019c. Increase in Surface Friction Dominates the Observed Surface Wind Speed Decline during 1973–2014 in the Northern Hemisphere Lands. J. Climate 32, 7421-7435. DOI: 10.1175/JCLI-D-18-0691.1.

Zhang, L., Traore, S., Cui, Y., Luo, Y., Zhu, G.e., Liu, B.o., Fipps, G., Karthikeyan, R., Singh, V., 2019a. Assessment of spatiotemporal variability of reference evapotranspiration and controlling climate factors over decades in China using geospatial techniques. Agricult. Water Manage. 213, 499–511.

Zhang, Q., Gu, X., Singh, V.P., Kong, D., Chen, X., 2015. Spatiotemporal behavior of floods and droughts and their impacts on agriculture in China. Global Planet. Change 131, 63–72.

Zhao, D., Zheng, D.u., Wu, S., Wu, Z., 2007. Climate changes in northeastern China during last four decades. Chin. Geogr. Sci. 17 (4), 317–324.

Zhao, Z.C., et al., 2016. Possible reasons of wind speed decline in China for the last 50 years. Adv. Meteorol. Sci. Technol. 6 (3), 106–109 (in Chinese).

Zuo, D., Cai, S., Xu, Z., Peng, D., Kan, G., Sun, W., Pang, B.o., Yang, H., 2019. Assessment of meteorological and agricultural droughts using in-situ observations and remote sensing data. Agricult. Water Manage. 222, 125–138.